JOURNAL OF GEOPHYSICAL RESEARCH, VOL. 114, G02015, doi:10.1029/2008JG000841, 2009

Interactions between soil thermal and hydrological dynamics in the response of Alaska ecosystems to fire disturbance

Shuhua Yi,[1,2] A. David McGuire,[3] Jennifer Harden,[4] Eric Kasischke,[5] Kristen Manies,[4] Larry Hinzman,[6] Anna Liljedahl,[6] Jim Randerson,[7] Heping Liu,[8] Vladimir Romanovsky,[9] Sergei Marchenko,[9] and Yongwon Kim[6]

Received 4 August 2008; revised 13 February 2009; accepted 5 March 2009; published 23 May 2009.

[1] Soil temperature and moisture are important factors that control many ecosystem processes. However, interactions between soil thermal and hydrological processes are not adequately understood in cold regions, where the frozen soil, fire disturbance, and soil drainage play important roles in controlling interactions among these processes. These interactions were investigated with a new ecosystem model framework, the dynamic organic soil version of the Terrestrial Ecosystem Model, that incorporates an efficient and stable numerical scheme for simulating soil thermal and hydrological dynamics within soil profiles that contain a live moss horizon, fibrous and amorphous organic horizons, and mineral soil horizons. The performance of the model was evaluated for a tundra burn site that had both preburn and postburn measurements, two black spruce fire chronosequences (representing space-for-time substitutions in well and intermediately drained conditions), and a poorly drained black spruce site. Although space-for-time substitutions present challenges in model-data comparison, the model demonstrates substantial ability in simulating the dynamics of evapotranspiration, soil temperature, active layer depth, soil moisture, and water table depth in response to both climate variability and fire disturbance. Several differences between model simulations and field measurements identified key challenges for evaluating/improving model performance that include (1) proper representation of discrepancies between air temperature and ground surface temperature; (2) minimization of precipitation biases in the driving data sets; (3) improvement of the measurement accuracy of soil moisture in surface organic horizons; and (4) proper specification of organic horizon depth/properties, and soil thermal conductivity.

Citation: Yi, S., et al. (2009), Interactions between soil thermal and hydrological dynamics in the response of Alaska ecosystems to fire disturbance, *J. Geophys. Res.*, *114*, G02015, doi:10.1029/2008JG000841.

1. Introduction

[2] Soil temperature is considered one of the most important environmental factors affecting soil organic matter decomposition [*Davidson and Janssens*, 2006]. In ecosystem models, decomposition of soil carbon is usually described as an exponential response with temperature. Soil moisture is also an important environmental factor as very low and very high soil moisture inhibit soil microbial activities, and thus decomposition [*Robinson*, 2002]; decomposition in soil carbon is maximized when soil moisture is between 50% and 75% volumetric soil moisture content [*Wickland and Neff*, 2007]. Northern high-latitude terrestrial ecosystems (arctic tundra and boreal forest) have accumulated more than 40% of global soil carbon because of cold and wet soils [*Tarnocai*, 2000]. This soil carbon storage is vulnerable as high latitudes are expected to experience more pronounced warming than other regions of the globe during the next century [*ACIA*, 2004]. In addition to an increase of soil temperature in a warming climate, permafrost, defined as ground (soil or rock) that remains at or below 0°C for at least 2 consecutive years, is vulnerable to degradation. Once thawed, the soil carbon previously protected at depth in frozen soils is subject to decomposition [*Goulden et al.*, 1998]. Changes in soil temperature and soil moisture can also affect nutrient

[1]Institute of Arctic Biology, University of Alaska Fairbanks, Fairbanks, Alaska, USA.
[2]Now at State Key Laboratory of Cryosphere Sciences, Cold and Arid Regions Environmental and Engineering Institute, Chinese Academy of Sciences, Lanzhou, China.
[3]Alaska Cooperative Fish and Wildlife Research Unit, U.S. Geological Survey, University of Alaska Fairbanks, Fairbanks, Alaska, USA.
[4]U.S. Geological Survey, Menlo Park, California, USA.
[5]Department of Geography, University of Maryland, College Park, Maryland, USA.
[6]International Arctic Research Center, University of Alaska Fairbanks, Fairbanks, Alaska, USA.
[7]Department of Earth System Science, University of California, Irvine, California, USA.
[8]Department of Physics, Atmospheric Sciences and General Sciences, Jackson State University, Jackson, Mississippi, USA.
[9]Geophysical Institute, University of Alaska Fairbanks, Fairbanks, Alaska, USA.

0148-0227/09/2008JG000841$09.00

availability [*van Cleve et al.*, 1983] and plant phenology [*van Wijk et al.*, 2003].

[3] There are two primary ways in which soil moisture can influence soil thermal dynamics: (1) the thermal conductivity of a dry organic soil (i.e., organic soil horizon composed of greater than 18% organic C) is substantially lower than that of a wet organic soil, which makes dry organic soil a good heat insulator [*Yi et al.*, 2007]; (2) the seasonal amplitude of soil temperature is damped through the release and absorption of latent heat. Conversely, the thermal state of soil can also influence hydrology: (1) frozen soils have limited infiltration capacity, which results in a large runoff during spring snowmelt [*Shanley and Chalmers*, 1999]; and (2) the base flow depends on the extent of unfrozen soil in the hydrologically active zone. For example, deeper unfrozen soil layers are thought to contribute to an increase in winter discharge from rivers flowing into the Arctic Ocean [*Oelke et al.*, 2004]. The interactions between soil thermal and hydrological dynamics are generally implemented in third generation land surface models, which are used in general circulation models to simulate the lower boundary water, heat and momentum fluxes [*Verseghy*, 1991; *Bonan*, 1996; *Oleson et al.*, 2004]. However, these interactions are generally neglected in most large-scale ecosystem models where one or two soil layers are used to simulate soil moisture dynamics in ecosystem models [e.g., *Sitch et al.*, 2003], and analytical or empirical functions are used for simulating soil thermal dynamics [e.g., *Bond-Lamberty et al.*, 2005]. Large-scale ecosystem models have considered vertical soil thermal dynamics (e.g., the Terrestrial Ecosystem Model, TEM [*Zhuang et al.*, 2001, 2002, 2003; *Euskirchen et al.*, 2006]), or the effects of soil moisture on biogeochemical dynamics [e.g., *Zhuang et al.*, 2004], but have not fully included a coupling between soil thermal and vertical soil moisture regimes.

[4] The active layer is the top portion of the soil that thaws during summer and freezes again during autumn in permafrost regions. Most physical, chemical and biological processes happen in the active layer. A change in active layer depth (ALD) may have substantial implications for ecosystem carbon balance [*Goulden et al.*, 1998]. The position of water table is an important indicator of soil wetness, and water table depth (WTD) is an important control on soil carbon decomposition [*Dunn et al.*, 2007]. Wildfire disturbances and drainage are important factors that influence soil thermal and hydrological regimes to affect ALD and WTD [*Harden et al.*, 2000, 2006]. Wildfire not only reduces the thickness of organic horizons, but also alters the surface properties [*Liu and Randerson*, 2008]. Soil drainage not only affects the hydrological dynamics of soil directly, but also influences the soil thermal dynamics indirectly through effects on the thickness of organic horizons that result from the responses of ecological processes and fire disturbance to drainage [*Harden et al.*, 2006]. For example, poorly drained ecosystems usually have thicker organic horizons than well drained ecosystems because they experience less frequent and less severe fires [*Harden et al.*, 2000]. However, the effects of drainage and wildfire are seldom considered in the simulation of soil temperature, active layer, soil moisture, and water table dynamics by ecosystem models [see *Zhang et al.*, 2002; *Bond-Lamberty et al.*, 2007; *Ju and Chen*, 2008].

[5] In this study, we use a process-based modeling approach to investigate interactions between soil thermal and hydrological dynamics in the response of Alaska ecosystems to fire disturbance. Such an approach requires a modeling framework that incorporates the interactions among organic horizon thickness and properties, soil temperature, and soil moisture into an ecosystem model. It is the main goal of this paper to build on the progress of previous versions of the Terrestrial Ecosystem Model (TEM) as represented by *Zhuang et al.* [2002, 2004] to (1) incorporate different types of organic horizons, i.e., live moss, and fibrous and amorphous organic horizons, into the soil structure; (2) differentiate the effects of drainage by incorporating two broad drainage classes, i.e., moderately well drained and poorly drained; and (3) develop and evaluate an efficient and stable numeric scheme for simulating soil thermal and hydrological dynamics within heterogeneous soil. We used the new version of TEM to investigate the following questions: (1) What is the effect of organic horizon thickness on soil thermal and hydrological dynamics? and (2) How does soil drainage influence interactions between soil thermal and hydrological dynamics? To address these questions we conducted a sensitivity analysis of how modeled active layer depth and water table depths responded to changes in important parameters and atmospheric driving data.

2. Methods

2.1. Background and Overview

[6] The Terrestrial Ecosystem Model (TEM) is a process-based ecosystem model designed to simulate the carbon and nitrogen pools of vegetation and soil, and carbon and nitrogen fluxes among vegetation, soil, and atmosphere [*Raich et al.*, 1991]. While previous model development efforts have improved the soil thermal and hydrological processes in TEM for application in high-latitude regions [*Zhuang et al.*, 2001, 2002, 2003, 2004; *Euskirchen et al.*, 2006], soil thermal and hydrological processes are not comprehensively coupled, and fire disturbance reduced the amount of soil carbon without affecting organic soil thickness and associated changes in the thermal and hydrological properties of organic soil [e.g., see *Balshi et al.*, 2007]. *Zhuang et al.* [2002] conducted model experiments that demonstrated that changes in organic matter horizons during and after fire potentially have important influences on soil temperature and moisture, but subsequent modeling efforts have not dealt with the issue of dynamic changes in organic horizons. Therefore, the model development research reported here is focused on the explicit coupling of soil thermal and hydrological processes in the context of a changing organic horizon, which is a necessary step toward dynamically simulating how changes in organic matter horizons during and after fire influence the interactions among soil thermal, hydrologic, and biogeochemical processes.

[7] In this study, we first describe the new environmental module (hereafter EnvM) that is responsible for simulating soil thermal and moisture dynamics in the dynamic organic soil framework of TEM (DOS-TEM). We then describe the field sites that were used to evaluate the EnvM. We also describe the information required for the operation of the

Table 1. Description of Sites Used in This Study

	Location	Major Vegetation	Mineral Soil	Latest Burn	References
K2	Kougarok, Seward Peninsula (65°25′N, 164°38′W)	Tussock tundra	loess	2002	*Liljedahl et al.* [2007]
FBKS	Fairbanks (64°52′N, 147°51′W)	Black spruce	loess	na	*Kim et al.* [2007]
DFTC	Twelve mile Creek, near Delta Junction (63°54′N, 145°40′W)	Black spruce	Silty loams over sand and gravel	~1920	*Manies et al.* [2004]
DFT87	As DFTC	Aspen	As DFTC	1987	As DFTC
DFT99	As DFTC	Black spruce	As DFTC	1999	As DFTC
DFCC	As DFTC	Black spruce	Loess overlying glacial till and outwash	~1885	*Harden et al.* [2006]
DFC99	As DFTC	Black spruce	As DFCC	1999	As DFCC

EnvM including site-specific parameters and atmospheric driving data. We then describe the validation data used to evaluate the model and the sensitivity analyses we conducted to better understand interactions between soil thermal and hydrological dynamics that are influenced by fire disturbance and soil drainage.

2.2. Model Development

[8] The detailed descriptions of the water and energy fluxes among the atmosphere, canopy, snow and soil, and within the soil are provided in Appendices A–E. In the EnvM, the ground surface is represented by a snow horizon, three soil organic horizons, two mineral soil horizons, and a rock horizon. Each horizon is further divided into layers that are explicitly treated with respect to energy and moisture exchange. For example, the snow horizon can consist of up to five snow layers.

[9] The organic soil horizons include live moss, fibrous organic soil, and amorphous organic soil. For accurate simulation of soil temperature and moisture, the soil horizons near the surface are divided into thin layers (e.g., layers are a few centimeters thick in the live moss horizon), and layers become thicker as the distance from the surface gets deeper (e.g., layers are approximately 10 m thick in the rock horizon). The number of layers is variable among the three organic soil horizons, which can consist up to 7 layers.

[10] Following the method used in land surface models, e.g., the Canadian Land Surface Scheme [*Verseghy*, 1991], the EnvM considers upper and lower mineral soil horizons. Each mineral soil horizon is 1 of 11 mineral soil types as defined by *Beringer et al.* [2001]. The upper mineral soil horizon consists of 2 layers with thicknesses of 10 and 20 cm. The lower mineral soil horizon consists of 3 layers with thickness of 50, 100, and 200 cm. Thus, the total thickness of the mineral soil is 3.8 m in EnvM. The rock horizon consists of 5 layers. The total thickness of the soil and rock horizons is around 50 m.

[11] During model simulations, a freeze-thaw front, using Stefan's algorithm, is introduced into each layer to overcome computational problems associated with heterogeneous thicknesses of the layers. Each layer can contain an unlimited number of fronts. The temperature of each layer is updated daily, and the phase changes can only happen in layers of the snow and soil horizons. The water content can only be updated in layers for which the temperature is above 0°C. Each model run spans 1901–2006, with the years before 1999 used for model spin-up.

2.3. Description of Sites Used for Model Evaluation

[12] Data from seven sites in Alaska were used to evaluate the EnvM in this study (Table 1): a tussock (*Eriophorum vaginatum*) tundra site located at Kougarok (K2) on the Seward Peninsula; a poorly drained black spruce (*Picea mariana*) site (FBKS) located near Fairbanks, Alaska; and two black spruce fire chronosequences located in Donnelly Flats near Delta Junction, Alaska (DFTC, DFT87, and DFT99; DFCC and DFC99), which represent well drained (DFTC, DFT87, and DFT99 sites) and intermediately drained (DFCC and DFC99 sites) conditions. The K2 site, which is located in an area of transition between continuous and discontinuous permafrost, experienced a severe to moderate burn in 2002, which removed 7–9 cm of organic soil between the *Eriophorum vaginatum* tussocks [*Liljedahl et al.*, 2007]. The K2 site is unique in that it has soil temperature and moisture measurements obtained from the same location both before and after the fire [*Liljedahl et al.*, 2007].

[13] The FBKS site, which is located on the campus of the University of Alaska Fairbanks, is a poorly drained black spruce forest. The dominant overstory vegetation is *Picea mariana* with a forest floor that is a mixture of tussocks, vascular plants, shrubs, *Spaghnum* moss, feather mosses, and lichen. These plants include *Betula glandulosa, Ledum palustre, Vaccinium vitis-ideae, Carex lugens, Sphagnum spp., Hylocomium splendens, Thuidium abietinum, and Cladina stellaris* [*Kim et al.*, 2007]. There is about 50 cm of organic soil overlying loess, with 8 cm of feather and *Sphagnum spp*. mosses on top of the organic soil.

[14] The DFTC, DFT87, and DFT99 sites are part of a well drained fire chronosequence located in Donnelly Flats, which is near Delta Junction, Alaska; with the most recent stand replacing fires in ~1920, 1987, and 1999, respectively [*Liu and Randerson*, 2008]. The tower control site in Donnelly Flats, DFTC, has an overstory of mature 80-year old black spruce trees and an understory dominated by feathermoss (*Hylocomium splendens, Pleurozium schreberi, and Aulacomnium spp.*) and lichen (genera: *Cetraria, Cladonia, Cladina, and Peltigera*). We treat the Donnelly Flats Tower Control (DFTC) site as the control site for nearby sites that burned in 1987 (DFT87) and in 1999 (DFT99). The DFT87 site has a heterogeneous overstory of aspen (*Populus tremuloides*) and willow (*Salix spp.*) with patches of moss (*Ceratodon purpureus and Polytrichum spp.*) in open areas; this vegetation is typical of black spruce forests that experience a severe fire in which most of the surface

Table 2. Projected Leaf Area Index, From January to December, of the Different Sites Simulated in This Study[a]

	K2	DFTC/DFCC/FBKS	DFT99/DFC99	DFT87
Jan	0.52	1.1	0.05	0
Feb	0.52	1.15	0.05	0
Mar	0.52	1.2	0.05	0
Apr	0.52	1.2	0.05	0.5
May	0.52	1.3	0.05	0.8
Jun	0.52	1.9	0.05	1.8
Jul	0.52	2	0.05	2.5
Aug	0.52	2	0.05	2
Sep	0.52	1.5	0.05	1.5
Oct	0.52	1.3	0.05	1
Nov	0.52	1.15	0.05	0
Dec	0.52	1.15	0.05	0

[a]Based on *Beringer et al.* [2005] for K2, TEM simulations for the DFTC, DFCC, and FBKS sites, an assumption of 0.05 for the DFT99 and DFC99 sites, and satellite data for the DFT87 site.

organic horizons are consumed [*Johnstone and Kasischke*, 2005]. The DFT99 site consists of standing dead black spruce boles killed by a fire in 1999. By 2002, ~30% of the surface at DFT99 was covered by grasses (*Festuca altaica*), evergreen shrubs (*Ledum palustre* and *Vaccinium vitis-ideae*), and deciduous shrubs (*V. uliginosum*). While the DFT99 site experienced a severe fire where most of the surface organic horizon had been removed by fire, recruitment of aspen seedlings was low, most likely limited by low soil moisture [*Kasischke et al.*, 2007].

[15] The DFCC and DFC99 sites are part of the intermediately drained fire chronosequence located in Donnelly Flats along Donnelly Creek. We treat the Donnelly Flats Creek Control (DFCC) site, which last burned in 1885, as the control site for DFC99, which burned in 1999. The ground cover is dominated by feather moss (*Hylocomium splendens, Pleurozium schreberi, and Aulacomnium spp.*) at DFCC and by the early successional postfire mosses *Ceratodon purpureus and Polytrichum spp.* at DFC99. These two sites were underlain by permafrost within 1 m of the soil surface at the time of the fire in 1999.

2.3.1. Site-Specific Input Parameters

[16] Site-specific parameters, including monthly projected leaf area index (LAI, Table 2) and organic soil thicknesses (Table 3), were used by EnvM in this study. For LAI of the K2 site, the value of 0.52 was used for all seasons based on *Beringer et al.* [2005]. The simulated monthly LAI from a previous version TEM for mature black spruce, which ranged from 1.1 to 2.0, were used for the DFTC, DFCC, and FBKS sites. For the DFT99 and DFC99 sites, we assumed that the LAI was 0.05 after the fire in 1999. The monthly LAI values of DFT87 were estimated based on satellite data [*Liu and Randerson*, 2008].

[17] The organic soil thicknesses were specified from field measurements of live moss, fibrous organic soil that includes dead moss or Oi horizons, and amorphous organic soil that includes mesic Oe or amorphous Oa horizons. For the K2 site, the soil organic horizons were 14 cm thick in year 2000, half of which was burned in 2002 [*Liljedahl et al.*, 2007]. At the FBKS site, the soil organic horizons are 50 cm thick. The mean thicknesses of organic horizons of the DFCC and DFTC sites are 20 and 10 cm, respectively. After the fires in 1999, only 10 and 3.5 cm organic soil remained at the DFC99 and DFT99 sites, respectively [*Manies et al.*, 2001, 2004]. The values in Table 3 for the Donnelly Flats sites represent the organic horizon thicknesses of the soil cores collected at the locations of soil moisture and temperature measurements.

[18] We used the measured fraction of fine root production at a black spruce site of the Bonanza Creek Long-term Ecological Research Program [*Ruess et al.*, 2006] to represent the root distribution used for estimating transpiration. Since we could not identify measurements of root distribution for aspen and tussock tundra in Alaska, the rooting distributions of balsam poplar and black spruce from *Ruess et al.* [2006] were used to specify root distributions for the DFT87 and K2 sites, respectively (Table 4). We assumed that there were no fine roots in the live moss horizon.

2.3.2. Atmospheric Driving Data

[19] The monthly climate data, including air temperature, precipitation, vapor pressure, and surface solar radiation, were retrieved from the Climate Research Unit (CRU) data sets [*Mitchell and Jones*, 2005] for the period 1901–2002. The CRU data sets do not include the period 2003–2006, so the anomalies of the National Center for Environmental Prediction (NCEP) reanalysis data sets [*Kanamitsu et al.*, 2002] were used to extend CRU data sets through 2006 [*Hayes et al.*, 2009]. For the period 1996–2006, the CRU-based atmospheric driving variables were replaced by site observations or nearby meteorological station measurements if they were available.

[20] For the K2 site, the mean monthly air temperature is about 10°C in summer and about −15°C in winter for the period 1999–2006 (Figure 1a). The precipitation in winter is around 20 mm/month and that of summer is around 36 mm/month (Figure 1d).

Table 3. Organic Horizon Thicknesses of the Different Sites Simulated in This Study

Site	Live Moss (cm)	Fibric Organic (cm)	Amorphous Organic (cm)	Total (cm)
K2	0.0 (0)[a]	4 (0)	10 (7)	14 (7)
FBKS	3	15	32	50
DFTC	2	10	10	22
DFT87	0.0	0.0	5.7	5.7
DFT99	0.0	0.0	3.5	3.5
DTCC	3	10	12	25
DFC99	0	4	9	13

[a]The data in parenthesis are for years after that burn at the K2 site.

Table 4. Percent of Fine Root Production in Each Depth Interval for the Top 1 m of Soil Below the Live Moss Horizon Based on *Ruess et al.* [2006]

Depth Interval (cm)	Black Spruce (%)	Balsam Poplar (%)
0–10	26.34	0.022
10–20	54.57	46.41
20–30	13.48	33.11
30–40	2.64	11.59
40–50	0.6	2.37
50–60	0.58	1.7
60–70	1.79	0.87
70–80	0	0.87
80–90	0	0.32
90–100	0	0.56

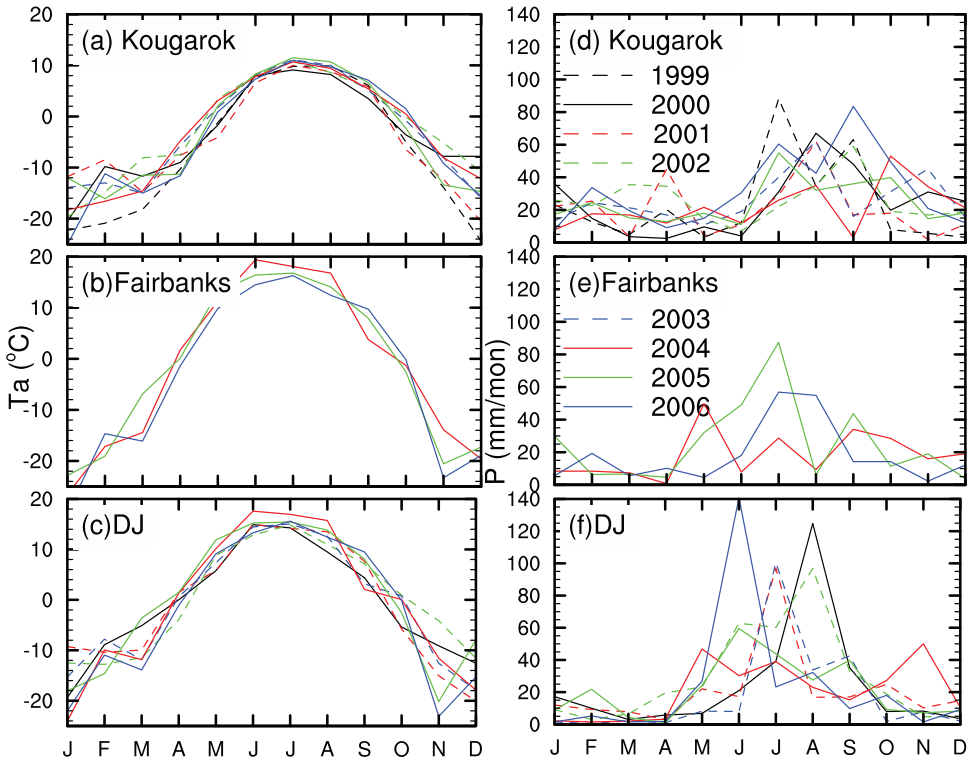

Figure 1. Monthly air temperature (Ta) and precipitation (P) of the Kougarok, on the Seward Peninsula, Fairbanks, and Delta Junction (DJ).

[21] For the Donnelly Flats sites, the mean monthly air temperature is about 15°C in summer and about −14°C in winter for period 2000–2005 (Figure 1c). The precipitation in winter is very low, around 10 mm/month, while in summer it is around 60 mm/month (Figure 1f). From January to March of 2003 and 2004, the monthly precipitation is nearly 0 mm. The atmospheric driving data for the Fairbanks site are similar to those of the Donnelly Flats sites (Figures 1b and 1e).

2.3.3. Implementation of the N Factor

[22] The N factor (n) is used to estimate temperature at the ground surface, either the soil surface or the snow surface, from atmospheric surface temperature [*Klene et al.*, 2001]. To our knowledge, snow surface temperature has never been measured for this purpose. Therefore, we defined as n to be 1.00 when snow is present. When snow is not present, we defined n as the ratio between thawing degree day sums of approximately 2 m air temperature and the ground surface. We found that n was 0.66, 0.94, and 1.10 for DFTC, DFT87 and DFT99, respectively, based on measured air temperature and surface soil temperatures. For the K2 site, n was assumed to be 1.00 since there were no measurements of ground surface temperature. For DFCC and DFC99, n was assumed to be 0.66 and 1.10, respectively, to be consistent with the stand age based estimates for DFTC and DFT99. Because the FBKS site is a mature black spruce site, we assumed that n was 0.66 to be consistent with the estimates for the other mature black spruce sites in the study.

2.3.4. Validation Data

[23] Eddy covariance measurements of water fluxes are available for DFT99, DFT87, and DFTC during the years 2002–2004. Seasonal variations and site differences in the closure of the surface energy balance were summarized by *Liu and Randerson* [2008]. In general, seasonal mean values of the closure ranged from 0.69 to 0.81 for the DFT99 site, from 0.75 to 0.86 for the DFT87 site, and from 0.71 to 0.87 for the DFTC site. The closure estimates are within the range of these reported by FLUXNET community [*Wilson et al.*, 2002]. These data were summed to daily resolution if there were more than 30 valid half-hour measurements in one day, otherwise, the daily water flux was considered as missing. Similarly, daily estimates were aggregated to make monthly estimates. The simulated monthly evapotranspiration, canopy evaporation, sublimation, transpiration, snow sublimation, and soil evaporation were summed and compared with the field-based estimates of water fluxes [*Liu and Randerson*, 2008] to evaluate the performance of the EnvM in estimating these water fluxes.

[24] Soil temperature and moisture measurements were available for all seven sites at different depths (2–100 cm) and for different periods (1999–2006). The soil temperature and moisture estimates were output from the EnvM at the same depth as each measurement for purposes of comparison. The thaw depth was measured approximately monthly using a permafrost probe at DFTC, DFT99, DFCC, and DFC99.

2.4. Sensitivity Analysis

[25] A sensitivity analysis was performed to investigate the effects of changes in parameters and driving data on model estimates for both a moderately well drained and a poorly drained black spruce forest. The baseline thicknesses of the live moss, fibrous organic and amorphous organic

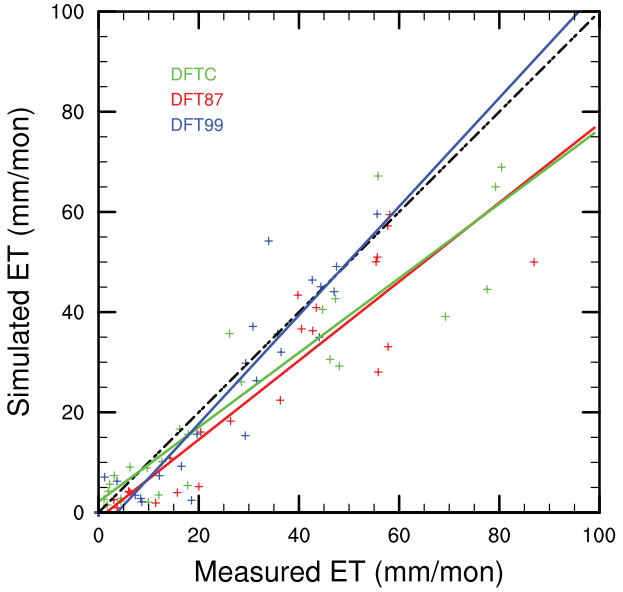

Figure 2. Scatterplots and linear regression lines of simulated and measured monthly evapotranspiration (ET) for the DFTC, DFT87, and DFT99 sites from 2002 to 2004.

horizons were set to 2, 7, and 5 cm for the moderately well drained forest, and to 3, 17, and 14 cm for the poorly drained forest based on the mean organic horizon thicknesses of black spruce stands in Manitoba, Canada [*Manies et al.*, 2006; *Yi et al.*, 2009] and Alaska [*Manies et al.*, 2003]. For the baseline simulation, the 2006 atmospheric driving data of the Donnelly Flats sites were used to run EnvM without changing any parameters. Changes to individual driving data inputs or parameters were then applied for each simulation of the sensitivity analysis. The input data and parameters considered in this sensitivity analysis are: atmospheric warm season temperature (i.e., monthly temperature > 0°C), snow, rain, surface solar radiation, organic soil thickness, LAI, topography factor, maximum drainage rate, minimum soil thermal conductivity, maximum snow density, snow albedo, and minimum soil evaporation ratio. The results of the equilibrium state after 100 years of simulation were analyzed in the sensitivity analysis.

[26] Because of the importance of active layer depth (ALD) and water table depth (WTD) on biogeochemistry of high-latitude terrestrial ecosystems, we focused the sensitivity analysis on evaluating the sensitivity of ALD and WTD to changes in the chosen input data and parameters. We evaluated the sensitivity of ALD and WTD using a sensitivity index similar to that used by *Friend et al.* [1993]. As an example, the sensitivity of ALD to air temperature (S_{ALD}) is defined as:

$$S_{ALD} = \frac{ALD_a - ALD_{bl}}{ALD_{bl}} \Big/ \left|\frac{Ta_a - Ta_{bl}}{Ta_{bl}}\right|$$

where ALD_{bl} is the simulated baseline ALD which used Ta_{bl} as the baseline air temperature driver and ALD_a is the simulated ALD using the Ta_a as the altered air temperature driver. Here the absolute value of the relative change in air temperature is used so that the sensitivity index provides information on whether ALD increased or decreased.

3. Results

3.1. Evapotranspiration

[27] The monthly field-based estimates of evapotranspiration (ET), which were available for sites of the tower chronosequence from 2002 to 2004, were substantially different among the DFTC, DFT87, and DFT99 sites (Figure 2). The simulated ET explained 80, 89, and 83% of the variability of the field-based ET estimates for the DFTC, DFT87 and DFT99 sites, respectively. The slope of the regressions between simulated and observed was less than 1 for both the DFTC and DF87 sites because of underestimation of ET in summer (Figure 2). The intercepts of the regressions between simulated and observed were not different from 0 at any of the three sites. See Table S1 in the auxiliary material for more detail.[1]

3.2. Freezing and Thawing Fronts

[28] In the EnvM, the freeze-thaw fronts were explicitly simulated using the Stefan algorithm. At the K2 site, the simulated prefire ALD reached 0.8 m in 2001 (Figure 3a). ALD measured at the nearby circumpolar active layer monitoring (CALM) network [*Brown et al.*, 2000] site was 0.56 ± 0.14 cm in 2001. In 2002, half of the 14 cm organic soil horizons at the K2 site was lost in the fire, and in 2003, the simulated ALD is more than 1.3 m. Both the reduction of organic soil horizons and warmer summer air temperature at the K2 site (Figure 1a) contributed to the deeper ALD in 2003.

[29] The simulated maximum ALDs of DFTC and DFT99 in 2001 were around 0.65 and 1.8 m, respectively (Figures 3c and 3d). Similarly, the simulated maximum ALD at the DFCC and DFC99 sites are about 0.6 m and 1.4 m, respectively (Figures 3e and 3f). The simulated and seasonal ALDs agree well at DFTC and DFCC in all months except September (Figures 3c and 3e) The ALD in September is underestimated at DFTC and overestimated at DFCC, however, the simulation is within 1 standard deviation of measurement, 37 and 11 cm for DFTC and DFCC, respectively. At the recently burned sites, DFT99 and DFC99, the simulated thaw depth is similar to the observed thaw depth in April and May, but is deeper than observed in June, July, and September (Figures 3d and 3f), The accurate measurement of thaw depth at these sites in July, August, and September was constrained by the existence of shallow gravel layer that prevented the permafrost probe from penetrating deeper. Soil pits excavated shortly after the fire in 1999 indicated that the permafrost table at DFT99 and DFC99 were deeper than 2 m and 1 m, respectively [*Harden et al.*, 2006].

[30] Additional simulations were conducted for DFTC, DFT99, DFCC, and DFC99 with the assumption that n factor equals 1.00. The simulated ALDs are about 0.8, 1.5, 0.8, and 1.3 m for DFTC, DFT99, DFCC, and DFC99, respectively. Differences in organic soil depths between

[1] Auxiliary materials are available in the HTML. doi:10.1029/2008JG000841.

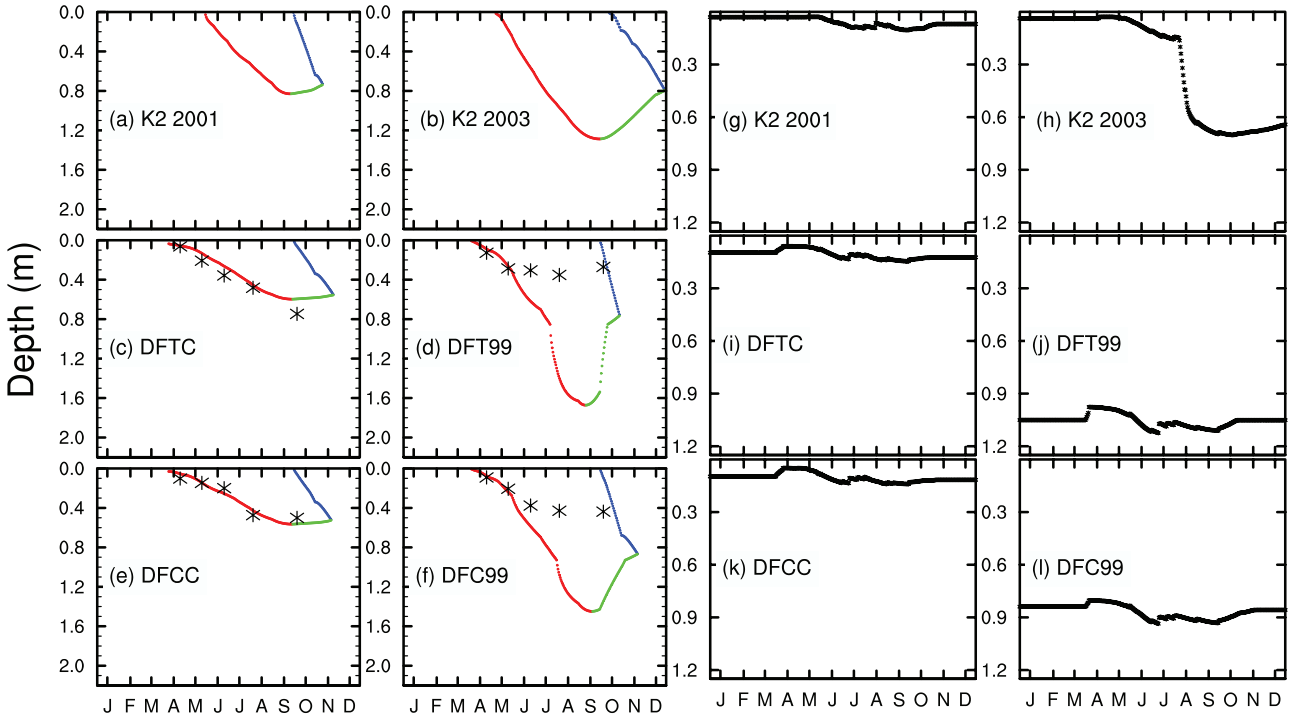

Figure 3. Simulated (a–f) freezing and thawing fronts and (g–l) water table depth for the K2 site before (2001) and after (2003) the fire in 2002, and for the DFTC, DFT99, DFCC, and DFC99 sites in 2001. The asterisks in Figures 3c–3f for the DFTC, DFT99, DFCC, and DFC99 sites represent the depth of the soil frost probe that attempted to measure thaw depth at the site. The red line represents the thawing fronts, the blue line represents the freezing front moving vertically downward from the surface, and the green line represents the freezing front moving upward toward the surface. The tick marks on the *x* axis represent the middle of each month.

DFTC and DF99 and between DFCC and DF99 were responsible for the ALD differences of 0.7 and 0.5 m between each pair of sites, respectively. Comparison of the differences in ALD between the mature and burned sites with an n factor of 1 versus the n factors we used revealed that approximately 60% of the differences can be explained by organic soil thickness. Thus, fire appears to be an important factor responsible for differences in ALD between mature and burned sites.

3.3. Soil Temperatures

[31] After updating the freeze-thaw fronts, the soil temperature is updated in the EnvM. We analyzed scatterplots of simulated and measured soil temperature at (1) all depths (Figure 4a), (2) shallow depths (~2 cm; Figure 4b), (3) intermediate depths (~25 cm; Figure 4c), and (4) deep depths (>38 cm; Figure 4d). On average, the model-based estimate of soil temperature explained more than 78% of variation in measured soil temperatures. At the K2 site, the slope of linear regressions between simulated and measured soil temperatures were not different from 1 (95% confidence interval) at each of the three depth comparisons; the intercepts were slightly negative but within 1.5°C of 0°C. At the FBKS site, while the slopes of the regressions are approximately 0.85, they are technically not significantly different from a slope of 1. However, the intercepts of the regressions at the FBKS site, which are approximately −3°C, are significantly less than 0°C. In general, the slopes

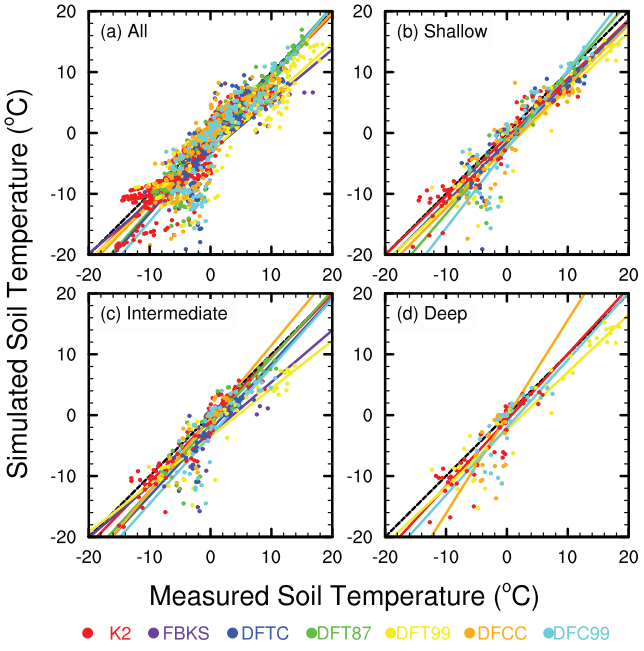

Figure 4. Scatterplots and linear regression lines of simulated and measured monthly soil temperatures for the K2, FBKS, DFTC, DFT87, DFT99, DFCC, and DFC99 sites for (a) all available soil layers, (b) shallow soil layers (2–4 cm), (c) intermediate soil layers (20–25 cm), and (d) deep soil layers (greater than 38 cm).

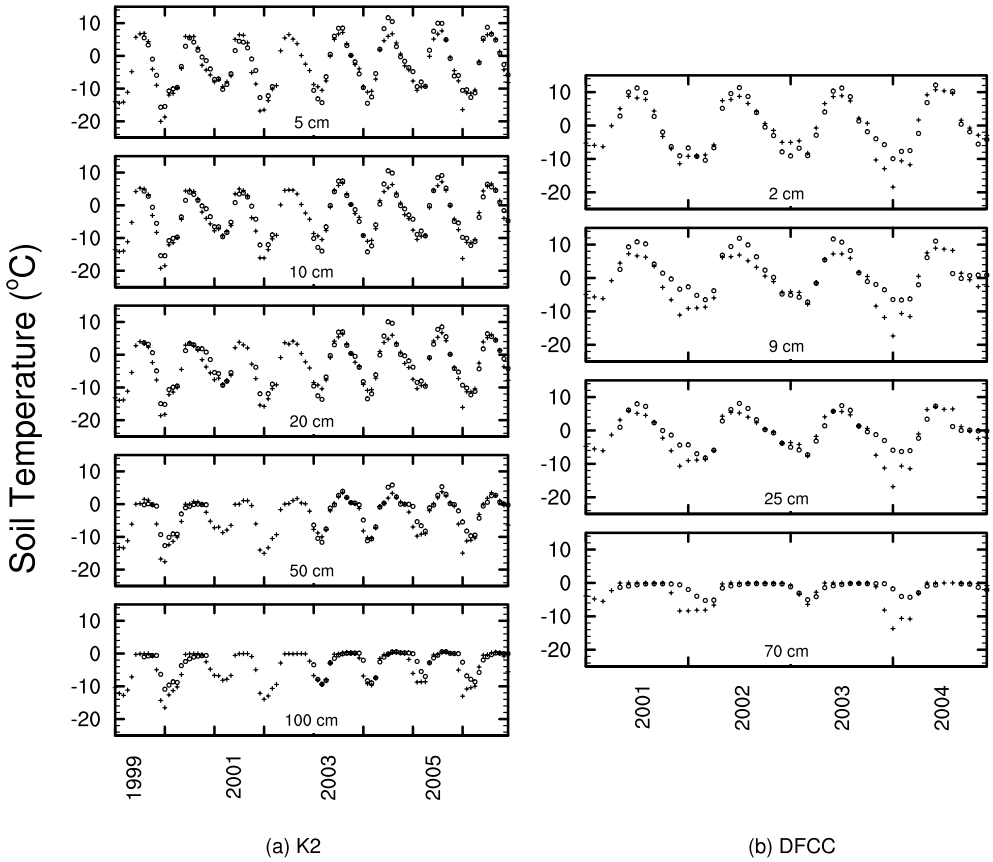

Figure 5. Comparisons between simulated (crosses) and measured (circles) monthly soil temperatures at different depths of the (a) K2 site from 1999 to 2006, at which fire occurred in 2002; and of the (b) DFCC site from 2001 to 2004.

of the regressions for the Donnelly Flats sites are not significantly different from 1. However, the range of the intercepts at the Donnelly Flats sites is between −0.5°C and −3.5°C, with most of the intercepts significantly less than 0°C. The negative intercepts are associated with underestimates of soil temperature that largely occur during winter. See Table S2 in the auxiliary material for more detail.

[32] The EnvM performed well in simulating soil temperature at the K2 site before the fire event in 2002, but underestimated the summer soil temperature (Figure 5a). It is possible that fire alters the surface characteristics, and that the n factor following fire may be greater than 1. At the Donnelly Flats sites, the EnvM underestimated soil temperatures during the winter of 2003–2004. The underestimation was about 6–10°C at the DFCC site (Figure 5b). In comparison to other winters reported in Figure 5b, the winter of 2003–2004 was characterized by substantially lower precipitation and colder atmospheric temperature in our driving data sets (Figures 1c and 1f). The simulated colder soil temperatures in the winter 2003–2004 are consistent with the climate data used to drive the simulations. In contrast, the measured soil temperature implies that the snowpack was thicker than in the other years, which is inconsistent with the precipitation in our driving data sets. Therefore, we suspect that the precipitation data are biased in 2003–2004 or that wind redistribution of snow results in similar snow depths at the sites in each year.

3.4. Water Table Depth

[33] As with the analysis of the simulated freeze-thaw fronts, we analyzed the simulated WTDs for the K2 site both before (2001) and after (2003) the fire (Figures 3g and 3h), and for the Donnelly Flats sites in 2001 (Figures 3i–3l). In the model simulation of the K2 site, the organic soil thickness was changed in August 2002. The WTDs at the K2 site increased to 70 cm in the following summer (Figure 3h), while those of 2001 are less than 10 cm. The increase of WTDs in 2003 is caused by the increase of ALDs, which are deeper than 1.3 m (Figure 3b). At the Donnelly Flats sites, the simulated WTDs decrease in April because of snowmelt infiltration. During the growing season, the simulated WTDs generally increase because of evapotranspirational water losses, but there are occasional decreases in WTD because of rainfall events. In general, the simulated WTDs of the mature forests (DFTC and DFCC) are shallower than those of the burned sites (DFC99 and DFT99) as deeper ALDs increase base flow at the burned sites.

3.5. Soil Moisture

[34] The soil moisture of each soil layer in the EnvM is updated immediately after soil temperature is updated. We analyzed scatterplots of simulated and measured soil temperature at (1) all depths (Figure 6a), (2) shallow depths (~2 cm; Figure 6b), (3) intermediate depths

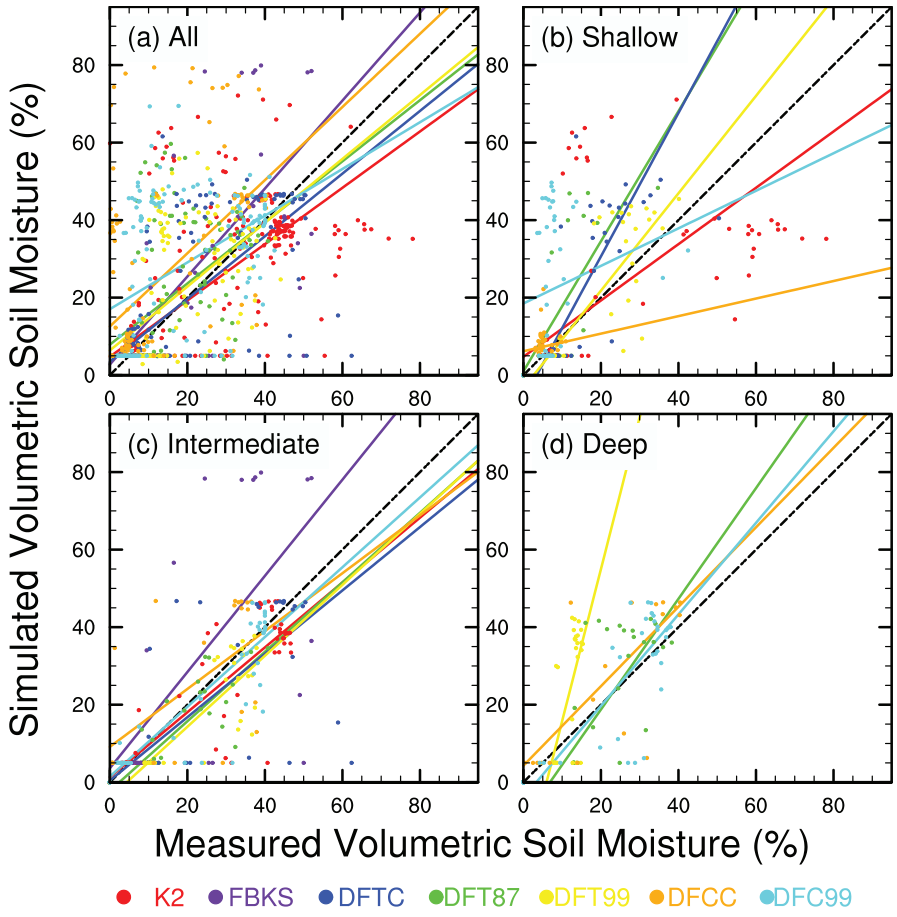

Figure 6. Scatterplots and linear regression lines of simulated and measured monthly soil moisture (volumetric water content, %) for the K2, FBKS, DFTC, DFT87, DFT99, DFCC, and DFC99 sites at (a) all available soil layers (all), (b) shallow layers (2–4 cm), (c) intermediate soil layers (20–25 cm), and (d) deep soil layers (greater than 38 cm).

(~25 cm; Figure 6c), and (4) deep depths (>38 cm; Figure 6d). In general, the correspondence between simulated and measured soil moisture is not as tight as the comparison between simulated and measured soil temperature. At the K2 site, the slope of linear regressions between simulated and measured soil moistures was significantly less than 1, with the slope highest (0.84) for the intermediate depth comparison, which was the only comparison in which the intercept was not significantly different from 0°C. At the FBKS site, the slopes of the regressions were not different than 1 and the intercepts were not significantly different from 0°C. At Donnelly Flats sites, the slopes of the regressions were generally not significantly different from 1 and the intercepts were generally not significantly different from 0°C. See Table S3 in the auxiliary material for more detail.

[35] The most successful simulations at all sites where those of the intermediate depths (~25 cm) (Figure 6c), which captured the seasonal variations (Figure 7). It is difficult to determine if the mismatches at shallow depths indicate problems with the model at shallow depths or are associated with biases in the measurements as it is very difficulty to accurately measure soil moisture in very porous organic soils [*Yoshikawa et al.*, 2004; *Overduin et al.*, 2005]. We suspect that the mismatches in the deeper soil layers are associated with uncertainties of representing lateral drainage in our simulations as the model assumes that lateral drainage only occurs in mineral soils at depths deeper than 80 cm. For the only very poorly drained site, FBKS, the simulated soil moistures are saturated at intermediate depth (30 cm), which are overestimated compared with observations (Figure 7). Several additional simulations were conducted for FBKS in which several parameters and driving variables were varied, but the results were not improved. The assumption of no lateral drainage in the organic soil horizons appears to not be valid for this site, which usually has ALD occurring in organic soil horizons. For moderately well drained sites, at intermediate depths, there are two notable types of differences between simulated and measured soil moisture. One is an artifact associated with the thermal timing of phase change in which the simulated increase in soil moisture lags the measured increase in soil moisture because the model assumes 5% volumetric unfrozen water content when soil is frozen, e.g., in the springs 2001 and 2002 at the DFTC site (Figure 7). The other difference is associated with improper representation of soil texture in the model, e.g., the porosity of the mineral soil at 25 cm of the DFTC site is specified to be less than 50%, but the measured volumetric water content for this site exceeded 60% in summer 2002.

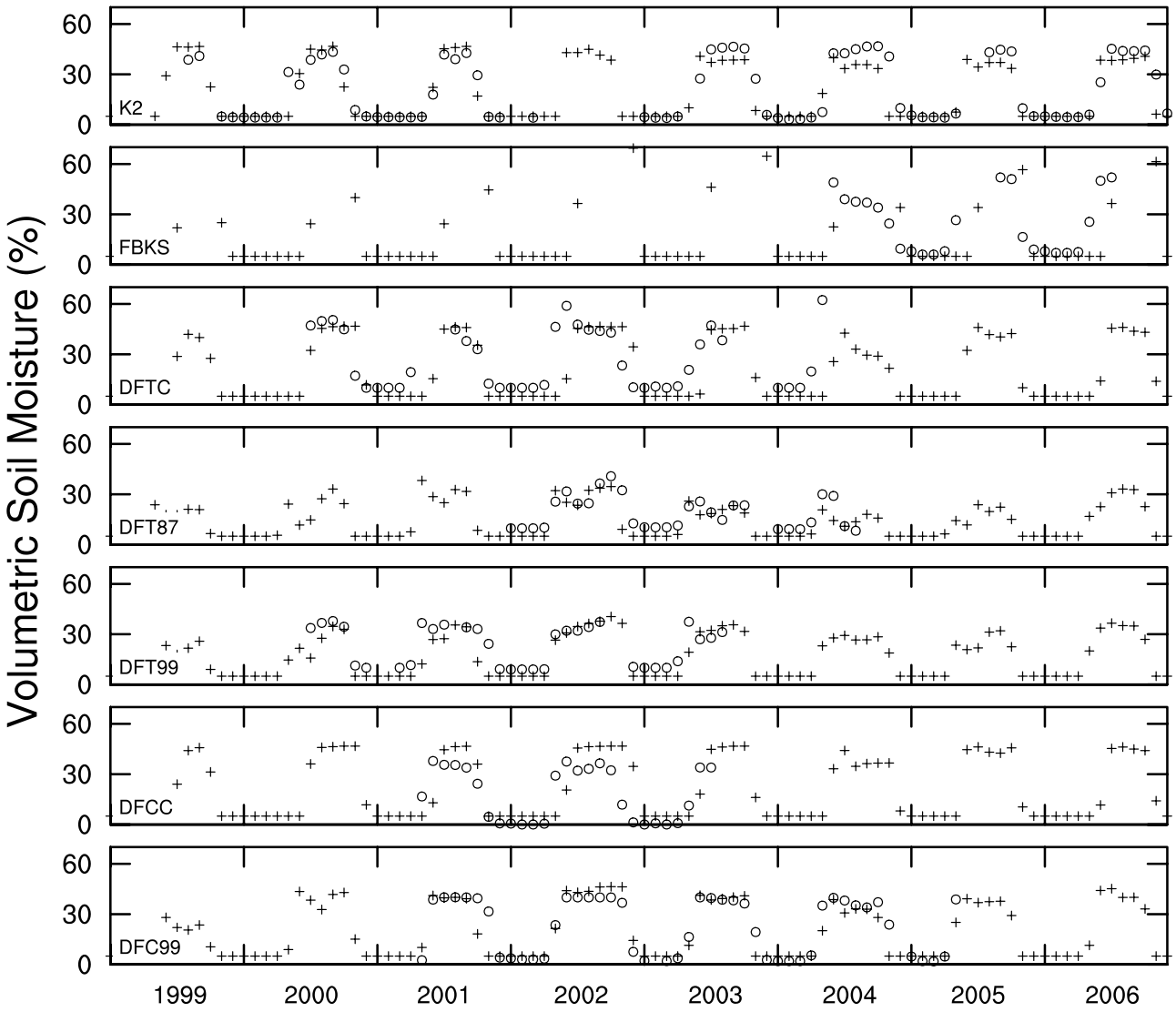

Figure 7. Comparisons between simulated (crosses) and measured (circles) mean monthly soil moisture at 20 cm for the K2 site, 30 cm for the FBKS site, and 25 cm for the DFTC, DFT87, DFT99, DFCC, and DFC99 sites from 1999 to 2006.

3.6. Sensitivity Analysis

[36] The ALD and WTD of the baseline simulation of the sensitivity analysis are 120 and 74 cm for the moderately well drained black spruce forest, respectively, and are 63 and 13 cm for the poorly drained black spruce forest. The sensitivity indices of ALD and WTD for the different simulations of the sensitivity analysis are plotted against each other in Figures 8a and 8b for the moderately well drained and poorly drained black spruce forests. The sensitivity of the ALD or WTD responses is represented by the distance of each point in Figures 8a and 8b from the origin; larger distances indicate greater sensitivity.

[37] Warm season air temperature (Ta), organic soil thickness (OS), and minimum soil thermal conductivity (TcSlMin) directly affect the thermal regime of soil (Figure 9). An increase of Ta or TcSlMin or a decrease of OS caused an increase of ALD and vice versa (Figures 8a and 8b). Increases of ALD cause increases of WTD for moderately well drained black spruce forest, due to the increases of base flow/drainage. But the change of WTD for poorly drained black spruce forest is small, since the base flow is set to 0. These differences are demonstrated in Figures 8a and 8b; the symbols in Figure 8b are more clustered near the vertical axis than those in Figure 8a.

[38] The role of subsurface drainage is also seen in contrasting responses of WTD to decreases in rain in which WTD of the poorly drained black spruce forest increases (see Figure 8b, region II), but WTD of the moderately well drained forest increases (see Figure 8a, region III). The decreased soil moisture associated with rain initially decreases the thermal conductivity of the soil, which causes a decrease in ALD (see both Figures 8a and 8b). In the moderately well drained forest the decrease in ALD results in less subsurface drainage (Figure 9), which decreases WTD. Because drainage is not affected by ALD in the poorly drained forest, the decrease in rain increases WTD.

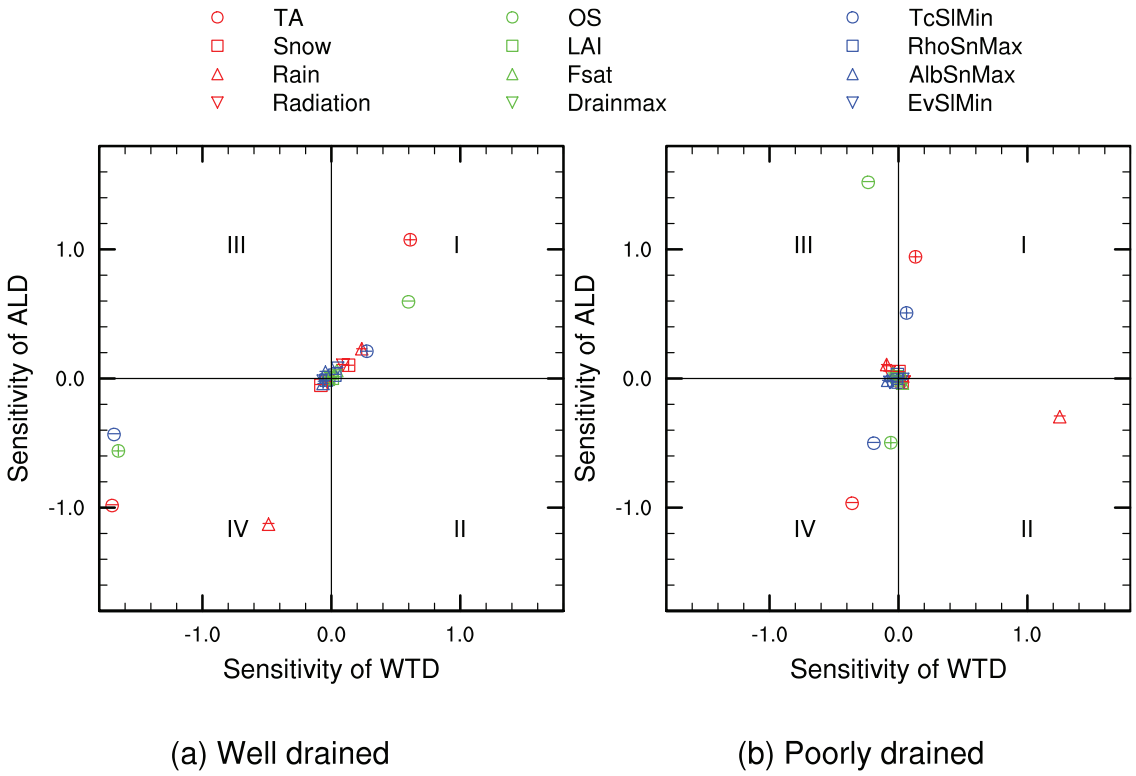

Figure 8. Sensitivity analysis results for a black spruce forest on (a) a moderately well drained soil and (b) a poorly drained soil. The factors to which active layer depth (ALD) and water table depth (WTD) are most sensitive are farthest from the zero-zero point. Plus and minus markers within the parameter symbols represent increases and decreases of the factor, respectively. Ta, summer atmospheric temperature; OS, organic soil thickness; LAI, leaf area index; Fsat, topography factor; DrainMax, maximum drainage rate; TcSlMin, minimum soil thermal conductivity; RhoSnMax, maximum snow density; AlbSn, snow albedo; EvSlMin, minimum soil evaporation fraction.

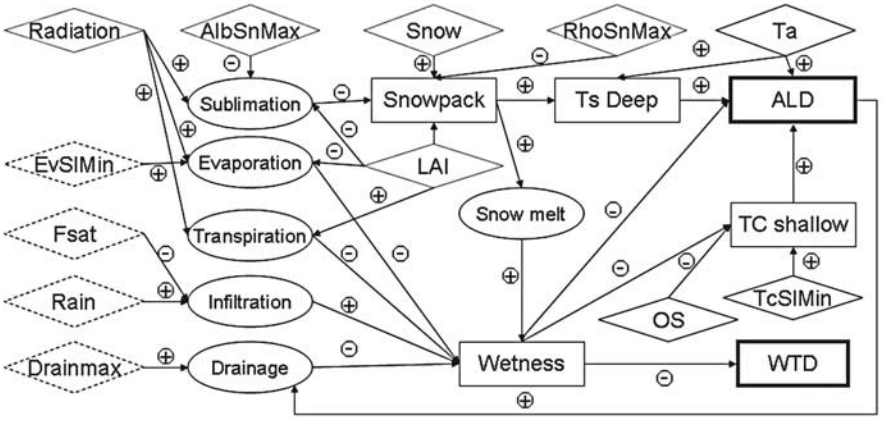

Figure 9. Relationships among the parameters/variables evaluated in the sensitivity analysis (diamonds), processes (ellipses), and states (rectangles). Evaporation, soil surface evaporation; sublimation, snowpack sublimation; Ts deep, deep soil temperatures; TC shallow, shallow soil thermal conductivity; other notation is the same as that used in Figure 8. The circled pluses (or minuses) mean that an increase of a parameter/variable at the beginning of the arrow will cause an increase (or a decrease) in the parameter/variable at the end of the arrow. Diamonds with dashed lines represent factors that directly affect water table depth (WTD); diamonds with solid lines represent factors directly affecting active layer depth (ALD). The remaining parameters/variables are included in diamonds with dotted lines. For clarity, the effects of ALD on transpiration are not shown here.

[39] The estimates of ALD and WTD simulated by the model were not responsive to changes in the other driving variables and parameters considered in the sensitivity analysis. One would expect that soil moisture would be affected by the surface evaporation ratio parameter (EvSlMin) and the topography parameter (Fsat). This insensitivity is caused by short-term self-adjustment of model, i.e., if infiltration is reduced by a decrease in EvSlMin, then the surface soil will become drier and there will be less runoff and more infiltration with the next rain event (Figure 9). Other factors we considered in the sensitivity analysis (radiation, LAI, and maximum snow albedo, AlbSnMax) have complex effects on the dynamics of the EnvM and involve negative feedback loops that result in low sensitivity of ALD and WTD (Figure 9). For example, as LAI increases ET will increase, which will tend to result in a drier soil. However, when the soil is drier, the surface infiltration becomes greater, which tends to result in a wetter soil. These negative feedbacks limit the effect of increasing LAI on WTD. Thus, while the model does not demonstrate substantial sensitivity to radiation, LAI, and maximum snow albedo, and AlbSnMax, these factors are still quite important in soil thermal and hydrological dynamics of the EnvM.

4. Discussion

[40] With respect to evaluating model performance in simulating responses to fire, the tundra (K2) site provided both preburn and postburn measurements to evaluate model performance. In contrast, the black spruce chronosequences represent space-for-time substitutions. While space-for-time substitutions have been a powerful means for studying progressive changes in ecosystems after a major disturbance [*Rastetter*, 1996], it is important to recognize that differences between sites of a chronosequence, for example differences in mineral soil chemistry and disturbance history, may result in comparisons that are not completely homologous with sites that have predisturbance and postdisturbance measurements. This aspect of space-for-time substitutions complicates model-data comparisons in which it is difficult to attribute whether model-data mismatches are associated with model performance issues or data quality issues. Even with these limitations to model-data comparison, the EnvM demonstrates substantial ability in simulating the dynamics of evapotranspiration, soil temperature, active layer depth, soil moisture, and water table depth in response to both climate variability and fire disturbance. The model is capable of simulating changes in active layer depth that affect water table depth through changes of subsurface drainage, changes that have the potential to influence biogeochemical dynamics. Our analyses also identified several differences between model simulations and field measurements that warrant attention. Below we discuss what we have learned from evaluation of the EnvM with respect to issues involving (1) atmospheric driving variables and (2) model parameters. We also briefly discuss the issue of soil moisture measurements in organic soils.

4.1. Issues Involving Atmospheric Driving Variables

[41] In our simulations, we used the estimates of daily air temperature and n factor to estimate ground surface temperature for purposes of estimating heat transferred between the ground and the atmosphere. The n factor, which is the ratio of temperature at the soil surface to that in the air, is used by some studies to estimate ground surface temperature from air temperature [*Klene et al.*, 2001; *Karunaratne and Burn*, 2004]. However, the n factor is affected by ground thermal properties and subsurface conditions [*Karunaratne and Burn*, 2004], and by vegetation cover [*Klene et al.*, 2001]. The n factor values reported in the literature range from 0.63 to 1.25 [*Klene et al.*, 2001]. Most ecosystem models do not use the n factor approach to estimate ground surface temperature and assume that ground surface temperature is the same as air temperature that is generally measured at 2 m height. We have used the n factor derived from the measurements at the sites analyzed in this study. Among the Donnelly Flats sites, the n factor is much greater at the recently burned sites than at the mature sites. At the K2 site, we assumed that the n factor of the burned site was equal to 1.00, which might represent an underestimate that could be responsible for the underestimation of summer soil temperatures following fire in 2002. Land surface models calculate ground surface temperatures through calculating ground surface energy balance based on subhour resolution of atmospheric driving data, (e.g., CLM3 [*Oleson et al.*, 2004]). Because ecosystem models generally use daily or monthly resolution atmospheric driving data, they cannot adequately make use of the methodology used in land surface models to calculate ground surface temperature. Given the sensitivity of ALD to air temperature identified in this study, some attention should be given to estimating more realistic ground surface temperature.

[42] The accuracy of precipitation data sets has been an important concern for applications of large-scale hydrological and ecosystem models in northern high-latitude regions [*McGuire et al.*, 2008] because of the low density of observations and numerous issues involved in accurately measuring snow fall [*Yang et al.*, 2005]. We believe that biases in precipitation or issues of redistribution of snow are responsible for some of the differences between simulated and measured soil temperature, e.g., the snow fall at the beginning of 2004 at Delta Junction is lower than snow fall at the beginning of the other years of our simulations.

4.2. Issues Involving Model Parameters

[43] The factors analyzed in the study can be broadly divided into three categories: (1) factors that directly affect ALD; (2) factors that directly affect WTD; and (3) factors that indirectly affect ALD and WTD through effects on various processes (Figure 9). Factors that directly affect ALD included warm season air temperature, minimum soil thermal conductivity, and organic soil thickness. An important dynamic identified in our analysis of the model simulations is that changes in ALD often affect WTD through changes of subsurface drainage. However, the strength of this effect depends on whether a site is well or poorly drained.

[44] In the sensitivity analysis we conducted, we did not evaluate all of the parameters in the model that affect hydrology. The parameters defining the hydraulic properties of moss, organic soil, and mineral soil can substantially affect the hydrological dynamics of the model. With respect to moss, there are two main types of bryophyte groups in boreal black spruce forests, feathermoss (e.g., *Hylocomium*

splendens), which generally occurs in well to intermediately drained conditions, and *Sphagnum*, which generally occurs in more poorly drained conditions [*Manies et al.*, 2006]. These moss types have distinct thermal, hydrological, and ecophysiological characteristics [e.g., see *Bisbee et al.*, 2001]. Feathermoss depends heavily on the precipitation and dew formation for water, while *Sphagnum* can wick water from deeper soil through capillary action. The soil moisture measurement at the FBKS site used in this study provides two data sets, one for soil pits with feathermoss cover, and the other with *Sphagnum* [*Kim et al.*, 2007]. The soil moisture at 30 cm of a "*Sphagnum* soil" is always greater than that of a "feathermoss soil." In this study we did not implement the different hydrologic properties of these different types of moss. It will be important to consider the distinct hydrological and thermal properties of different types of moss that occur in moderately well drained and poorly drained situations in future applications of the model.

[45] There are significant differences in hydraulic properties among different types of organic soil [*Letts et al.*, 2000]. *Beringer et al.* [2001] did not implement differences among different organic soils. We therefore defined porosities for moss, fibrous organic soil, and amorphous organic soil based on field measurements for black spruce forests in Manitoba, Canada [*Yi et al.*, 2009]. In addition to porosity, pore size distribution is another important factor affecting water movement in organic soils [*Clapp and Hornberger*, 1978; *Cosby et al.*, 1984]. If the same saturated hydraulic conductivity and pore size distribution are used for fibrous and amorphous organic soil, the fibrous organic soil with larger porosity would tend to suck water from the amorphous organic soil horizons below. However, amorphous organic soil usually has much larger values of the pore size distribution parameter than fibrous organic soil, which means that amorphous organic soil can hold water more tightly than fibrous organic soil. In this study, a larger value of pore size distribution (i.e., 6) has been used for the amorphous organic horizon than for fibrous organic horizon (4 based on *Beringer et al.* [2001]). The proper parameterization of different types of organic soil continues to be a key challenge in the simulation of soil water dynamics.

4.3. Issues of Soil Moisture Measurement

[46] A key challenge in evaluating the simulation of soil moisture is confidence in the accuracy and precision of the measurements of soil moisture. We found that the EnvM is better in simulating soil moisture at depth than in simulating soil moisture near the surface. It is currently very challenging to measure soil moisture in surface organic soils because the high porosity creates substantial difficulties in calibrating instruments used to measure soil moisture [*Yoshikawa et al.*, 2004; *Overduin et al.*, 2005]. The potential for substantial measurement error in field-based soil moisture estimates makes it difficult to ascertain what discrepancies between model- and field-based estimates require attention in the model.

5. Conclusion

[47] This paper presented and evaluated a stable and efficient scheme for incorporating the interactions of soil thermal and hydrological processes in a terrestrial ecosystem modeling framework. Our analysis using this framework revealed that changes in active layer depth often affect water table depth through changes of subsurface drainage. Because these changes have the potential to influence biogeochemical dynamics, we suggest that it is important for models of carbon dynamics in cold regions to more comprehensively represent interactions between soil thermal and hydrological processes.

[48] Key challenges identified in this study for evaluating/improving model performance include (1) proper representation of discrepancies between air temperature and ground surface temperature; (2) minimization of precipitation biases in the driving data sets; (3) improvement of the measurement accuracy of soil moisture in surface organic horizons; and (4) proper specification of organic horizon depth, hydrological properties, and soil thermal conductivity. Resolution of these observational issues will help in reducing model uncertainties. As changes in organic horizons caused by wildfire have substantial effects on soil thermal and hydrological regimes, an important next step is to investigate how the dynamics of organic soil thickness associated with wildfire disturbance and ecological succession affect the dynamics of permafrost and soil carbon in high latitudes.

Appendix A

[49] This part contains the detailed descriptions of the water and energy fluxes among the atmosphere, canopy, snow and soil, and within soil layers. In the environmental module (EnvM; Figure S1 in the auxiliary material), the ground layers include snow layers, soil layers, and rock layers. The soil layers include live moss, fibrous organic soil, amorphous organic soil, and mineral soil. Eleven mineral soil types have been considered in this study following *Beringer et al.* [2001]. The parameters of the EnvM are provided in Table A1.

A1. Estimation of Daily Atmosphere Driving Variables

A1.1. Incident Radiation

[50] The monthly short-wave irradiance incident on land surface (*NIRR*) is provided as input (W m^{-2}). Daily radiation is estimated from monthly values through linear interpolation.

A1.2. Air Temperature

[51] The daily air temperature (T_a) is derived from monthly values using linear interpolation.

A1.3. Precipitation

[52] The daily precipitation (mm/day) is downscaled from monthly precipitation (mm/month) based on the algorithm of *Liu* [1996], as used by *Zhuang et al.* [2004]. The daily precipitation is identified as rain when the daily air temperature greater than 0°C, otherwise it is identified as snow.

Appendix B: Effects of Vegetation on Radiation and Water Fluxes

B1. Radiation

[53] NIRR is divided into three components: reflectance back to the atmosphere, radiation intercepted by the canopy,

Table A1. Parameters Used in the Environmental Module of TEM[a]

	Name	Symbol	Unit	Value	Sources and Comments
			Parameters That Do Not Depend on Vegetation or Drainage		
Vegetation	VPD Start	VPD_{start}	Pa	930	Start of conductance reduction when vapor pressure deficit is lower than this value; *White et al.* [2000]
	VPD Close	VPD_{close}	Pa	4100	Stomata are closed when vapor pressure deficit is lower than this value; *White et al.* [2000]
	PPFD50	$PPFD_{50}$	μ mol $\times$ m^{-2} $\times$ s^{-1}	75	The radiation at which the stomata are 50% open; *White et al.* [2000]; used in Appendix B
Snow	Maximum Albedo	$\alpha_{sn,max}$	-	0.8	*Roesh et al.* [2001]; used in Appendix C
	Minimum Albedo	$\alpha_{sn,min}$	-	0.4	*Roesh et al.* [2001]; used in Appendix C
	Snow density of freshly fallen snow	$\rho_{sn,new}$	kg m^{-3}	120	*Verseghy* [1991]; used in Appendix E
Soil	Minimum thermal conductivity	$k_{sl,min}$	W $\times$ m^{-1} $\times$ K^{-1}	0.1	*Hinzman et al.* [1991]; used in Appendix E
	Minimum evaporation ratio	$E_{vr,min}$	-	0.15	See Appendix D
	Wilting point potential	Ψ_{max}	mm	-1.5×10^5	*Oleson et al.* [2004]; used in Appendix B
Rock	Thermal conductivity	k_r	W $\times$ m^{-1} $\times$ K^{-1}	2	*Clauser and Huenges* [1995]; used in Appendix E

	Name	Symbol	Unit	Dry	Wet	Sources and Comments
			Parameters That Depend on Drainage			
Soil	Maximum drainage rate	Drainmax	mm $\times$ s^{-1}	0.04	0	See Appendix D
	Topography parameter	Fsat	-	0.3	0.3	See Appendix D

	Name	Symbol	Unit	TUN	DEC	CON	Sources and Comments
			Parameters That Depend on Vegetation				
Vegetation	Albedo	α_v	-	0.19	0.19	0.1	*Beringer et al.* [2005]; used in Appendix B
	Boundary layer conductance	g_{bl}	mm $\times$ s^{-1}	0.04	0.01	0.08	The parameter for tundra is defined based on the C3 grass parameter of *White et al.* [2000]
	Cuticular conductance	g_c	mm $\times$ s^{-1}	0.00001	0.00001	0.00001	*White et al.* [2000]
	Maximum stomatal conductance	$g_{s,max}$	mm $\times$ s^{-1}	0.005	0.005	0.003	*White et al.* [2000]
Snow	Maximum snow density	$\rho_{sn,max}$	kg m^{-3}	362	250	250	Based on *Ling and Zhang* [2006] and *Pomeroy et al.* [1998]; used in Appendix E

[a]TUN, tundra; DEC, boreal deciduous forest; CON, boreal conifer forest; Dry, moderately well drained soil; Wet, poorly drained soil.

and radiation that is passed through the canopy and becomes incident on the ground surface.

B1.1. Radiation Reflectance to the Atmosphere (R_{v2a})

[54]

$$R_{v2a} = NIRR \cdot \alpha_v$$

where α_v is vegetation albedo. The albedos of tundra, deciduous, and conifer forest were assigned to be 0.19, 0.19, and 0.10, respectively [*Beringer et al.*, 2005].

B1.2. Radiation Through Canopy to the Ground (R_{v2g})

[55] Beer's law is used to calculate the extinction of radiation in canopy:

$$R_{v2g} = (NIRR - R_{v2a})e^{-E_R LAI}$$

where E_R (= 0.5) is a dimensionless extinction coefficient of radiation in the canopy. LAI is projected leaf area index.

B1.3. Radiation Intercepted by the Canopy (R_v)

[56]

$$R_v = NIRR - R_{v2a} - R_{v2g}$$

B2. Water

B2.1. Water Intercepted by the Canopy

[57] The calculations of rain ($W_{v,r}$) and snow ($W_{v,s}$) interception by the canopy are the same as those described in equations (A15) and (A16) of *Zhuang et al.* [2002].

B2.2. Water From the Canopy to the Atmosphere

[58] The overall water flux from the canopy to the atmosphere is calculated using the Penman-Monteith equation. The water flux consists of three components: (1) evaporation of canopy liquid water ($Q_{v,evp}$), (2) sublimation of canopy snow ($Q_{v,sub}$), and (3) transpiration ($Q_{v,trs}$). If there is intercepted rain or snow, the intercepted radiation (R_v) is first used to evaporate rain or sublimate snow. The remaining energy is then used to drive the transpiration formulation. The detailed equations for these fluxes are described in Appendix D of *Zhuang et al.* [2004]. Several modifications have been made for the calculation of stomatal conductance:

$$g_s = g_{s,\max} f(T_{\min}) f(VPD) f(PPFD) f(\Psi)$$

where g_s and $g_{s,\max}$ are the stomatal conductance and maximum stomatal conductance ($m \cdot s^{-1}$), and $f(T_{\min})$, $f(PPFD)$, and $f(\Psi)$ are the effects of minimum air temperature, radiation, and leaf water potential on stomatal conductance, respectively. The effect of $f(PPFD)$, which was not considered by *Zhuang et al.* [2004], was implemented in the EnvM following *Waring and Running* [1998]:

$$f(PPFD) = \frac{PPFD}{PPFD + PPFD_{50}}$$

where $PPFD$ is the absorbed solar radiation by canopy ($J \times m^2 \times s^{-1}$), and $PPFD_{50}$ is the value of $PPFD$ at which caused $f(PPFD)$ is 50% saturated. In this study, $PPFD_{50}$ is set to 75 μ mol $\cdot$ $m^{-2} \cdot s^{-1}$ or 16.5 $J \times m^2 \times s^{-1}$.

[59] With the vertical distribution of soil water content calculated, $f(\Psi)$ is modified to include the effects of root distribution on transpiration, following *Oleson et al.* [2004]:

$$f(\Psi) = \sum_i w_i r_i \geq 1 \times 10^{-10}$$

where w_i is plant wilting factor for layer i, and r_i is fraction of roots in layer i. The plant wilting factor w_i is calculated as:

$$w_i = \begin{cases} \dfrac{\Psi_{\max} - \Psi_i}{\Psi_{\max} + \Psi_{sat,i}} & T_i > 0 \\ 0 \quad T_i < 0 \end{cases}$$

where $\Psi_{\max}$ is a specified constant value for the wilting point potential of leaves (-1.5×10^5 mm), Ψ_i and $\Psi_{sat,i}$ are soil water matric potential and saturated matric potential (mm) of layer i (see Appendix D), and T_i is the soil temperature in layer i (°C).

B2.3. Water Fluxes From the Canopy to the Ground

[60] The water fluxes from the canopy to the ground consist of four components including throughfall of snow or rain, and the "dripping" of snow or rain from the canopy after throughfall. The throughfall fluxes of snow or rain are calculated as the precipitation input of snow or rain minus the interception of snow or rain. The "dripping" fluxes of snow or rain are calculated as the interception of snow or rain minus the sublimation or evaporation of snow or rain.

Appendix C: Effects of Snowpack on Radiation and Water Fluxes

[61] The snowpack is divided into a maximum of five layers, similar to the method used in CLM3 (Community Land Model, V3 [*Oleson et al.*, 2004]). The snowpack accumulates from the fluxes of snow throughfall and drip from the canopy, and it is subject to ablation from sublimation and melt. The dynamics of the snow layers are implemented using a double linked list structure, so that when a snow layer is too thin it is combined with an adjacent snow layer or it is removed if there is no adjacent snow layer. When a snow layer is too thick, it is divided into two snow layers. The criteria for the thickness range of snow layers are similar to those criteria used in CLM3.

C1. Radiation

[62] The radiation from the snowpack to the atmosphere is calculated as:

$$R_{sn2a} = R_{v2g} \cdot \alpha_{sn}$$

where α_{sn} is snow albedo, which is calculated following *Roesh et al.* [2001].

$$\alpha_{sn} = \alpha_{sn,\max} - (\alpha_{sn,\max} - \alpha_{sn,\min}) \frac{T_a + 10}{10}$$

$\alpha_{sn,\max} = 0.8$ and $\alpha_{sn,\min} = 0.4$ are maximum and minimum snow albedo.

C2. Water

C2.1. Water From the Canopy to the Snowpack

[63] The throughfall and drip of snow from canopy are added to snowpack.

C2.2. Water From the Snowpack to Atmosphere (Q_{sn2a})

[64] If air temperature is less than -1°C, then snowpack is sublimated using available radiation:

$$Q_{sn2a} = \left(R_{v2g} - R_{sn2a}\right)S_A/\left(L_{vap} + L_{fus}\right)$$

where $S_A = 0.6$ is snow absorptivity [*Zhuang et al.*, 2002], $L_{vap} = 2.51 \times 10^6$ J · kg^{-1} is the latent heat of vaporization, and $L_{fus} = 3.337 \times 10^5$ J · kg^{-1} is the latent heat of fusion.

C2.3. Water From Snowpack to the Soil

[65] If air temperature is greater than -1°C, snowpack can be melted by radiation or by heat conduction. The radiation-driven melt is calculated as:

$$Q_{sn2sl,rad} = \left(R_{v2g} - R_{sn2a}\right)/L_{fus}$$

The heat conduction-driven melt is described below in E.

Appendix D: Effects of Soil on Radiation and Water Fluxes

D1. Radiation

[66] The radiation from soil surface to atmosphere is calculated as:

$$R_{sl2a} = R_{v2g} \cdot \alpha_{sl}$$

where α_{sl} is soil albedo, which is calculated following the NCAR LSM [*Bonan*, 1996] using color classes related to soil types. The color class of moss is assigned to be 3 following *Beringer et al.* [2001], and the color classes of the fibrous and amorphous organic layers are assigned to be 8, which can be exposed by fire, the darkest class. The overall reflectivity of soil is considered to be the average of reflectivity of visible and near infrared radiation.

D2. Water

[67] The methods of the CLM3 are used to calculate the surface runoff and base flow [*Oleson et al.*, 2004]. The infiltration is estimated as the difference between input, i.e., rain and/or snowmelt, and runoff. If the topsoil layers (more than 2) are unfrozen, the finite difference equations are used to solve for the movement of water between layers, with the infiltration as top boundary condition, and zero drainage as the bottom boundary condition.

D2.1. Surface Runoff (Q_{over}) and Infiltration ($Q_{\mathrm{inf}\ l}$)

[68] Surface runoff (Q_{over}, mm · s^{-1}) is calculated following method of CLM3 [*Oleson et al.*, 2004]. The rest of input of water is considered as infiltration. Surface runoff is calculated based on the water table depth and fraction of saturation, which is determined by a topography parameter, Fsat. In this study, the default value from CLM3, 0.3, is used.

D2.2. Transpirational Loss of Soil Water

[69] On the basis of the fine root production fraction over soil profile, each soil layer loses soil water through transpiration. The sum of soil water lost to transpiration is equal to the transpirational flux calculated for the canopy (see Appendix B).

D2.3. Evaporation ($Q_{sl,evap}$) of Soil Water

[70] The calculation of potential evaporation ($Q_{sl,pe}$) from the soil surface is same as that described in Appendix A of *Zhuang et al.* [2002], which is based on the Penman equation. If the rain and snowmelt are greater than $Q_{sl,pe}$, the actual evaporation is calculated as:

$$Q_{sl,evap} = 0.6 \times Q_{sl,pe}$$

If rain and snowmelt are less than $Q_{sl,pe}$,

$$Q_{sl,evap} = E_{vr} \times Q_{sl,pe}$$

where E_{vr} is defined as $E_{vr} = \frac{0.3}{DSR^2}$, and DSR is the number of days since the last rain. However, experiments have shown that the evaporation from the soil surface is generally underestimated when downscaling precipitation from monthly values to daily values. Therefore, in this study a minimum evaporation ratio (0.08) is assigned, based on the observed water fluxes from DFT99 site, which was burned in 1999.

D2.4. Water Movement Between Soil Layers

[71] On the basis of the calculations of evaporation, infiltration, and transpiration, the movement of soil water between soil layers is calculated by solving Richards' equation. Because there are cases for which the updated soil water content of a soil layer can become negative or more than porosity at a daily time step, an iterative method is used to solve Richards' equation. The initial time step at beginning of each day is a half day. If after a time step any soil water content is not reasonable (negative or greater than porosity), then the time step is halved, and this continues until the solution is reasonable. The solution continues until a 1-day period is fully covered.

[72] The soil matric potential (ψ) and hydraulic conductivity (K) are calculated following *Clapp and Hornberger* [1978] and *Cosby et al.* [1984].

$$\psi = \begin{cases} \psi_{sat}\left(\dfrac{\theta_{liq}}{\theta_{sat}}\right)^{-b} & T_{sl} > 0 \\ 10^3 \dfrac{L_f}{g}\dfrac{T_{sl} - T_f}{T_{sl}} & T_{sl} \le 0 \end{cases}$$

where ψ_{sat} is saturated matric potential (mm), b is the *Clapp and Hornberger* [1978] constant, g is gravitational acceleration (m · s^{-2}), T_{sl} is soil temperature (K), and T_f is freezing point of liquid water (K).

$$K = K_{sat}\left(\frac{\theta_{liq}}{\theta_{sat}}\right)^{2b+3}$$

where K_{sat} is saturated hydraulic conductivity (mm $\cdot$ s^{-1}). ψ_{sat}, K_{sat}, and b are specified for each type of soil following *Beringer et al.* [2001].

D2.5. Base flow (Q_{bf})

[73] After the soil water contents of all layers are updated, the base flow is calculated following method of CLM3 [*Oleson et al.*, 2004]. Drainmax is an important parameter determining the maximum rate of drainage from unsaturated fraction, in this study, the default value of 0.04 mm/s, is used. In the CLM3, only the deep soil, 6–10 layers, has base flow. In this study, if the mineral soil layers, deeper than 80 cm, are unfrozen, then there can be base flow from these layers, otherwise the base flow is 0. For poorly drained soils, the base flow is assumed to be 0.

D2.6. Water Table Depth

[74] The WTD (depth from ground surface to groundwater surface, m) is calculated following the method of *Oleson et al.* [2004]:

$$WTD = z_{h,n} - \sum_{i=1}^{n} s_i \Delta z_i$$

where $z_{h,n}$ is the distance between soil surface and the bottom of soil layer n, s_i is soil wetness of soil layer n, and Δz_i is the thickness of soil layer n.

Appendix E: Soil Thermal Dynamics

[75] In previous versions of TEM, the Goodrich method was to solve for soil thermal dynamics [*Zhuang et al.*, 2001]. The Goodrich method first updates the soil/snow temperatures of layers above and below freezing/thawing fronts (FTFs), and assumes 0°C for layers between two FTFs, and then determines the positions of FTFs using updated temperatures. However, sometimes the Goodrich method cannot provide a valid solution for the position of FTFs, and thus the soil temperatures. This instability get worse when the soil thermal properties are coupled with soil water content. In EnvM, a stable snow/soil thermal model has been developed that, uses the Two-Directional Stefan Algorithm (TDSA) [*Woo et al.*, 2004]. The TDSA can satisfactorily simulate the positions of FTFs in a land surface model when proper surface forcing is provided [*Yi et al.*, 2006].

E1. Soil Freezing and Thawing Fronts

[76] In EnvM, the positions of FTFs are first determined at a daily time step using the TDSA. The TDSA first processes layers from top to bottom, using ground surface temperature as the forcing for the surface layer, until all the energy (degree days) is used up, or the front meet the bottom boundary of soil. The temperature at the bottom of first rock layer is then used as the forcing for the bottom boundary to force the deepest FTF upward; between September and April, the temperature at the bottom of last mineral layer is used instead. A FTF separates a layer into homogeneous frozen and unfrozen parts. The snow/soil column can be treated as a set of homogeneous frozen and unfrozen sublayers. Take a positive driving temperature in summer as an example. At the beginning of the TDSA:

$$dd_{left} = T_0 d$$

where T_0 is the ground surface temperature (°C), d is day, and dd_{left} is the available degree days for phase change (°C day).

[77] If a layer is frozen, then phase change will happen in this layer. TDSA calculates

$$dd_{need,i} = \theta_i \lambda d_i \left(R_{sum,i} + \frac{R_i}{2} \right)$$

where $dd_{need,i}$ is the degree day (°C day) needed to completely thaw layer i, θ_i is the volumetric water content of layer i (m^3/m^3), λ is latent heat of fusion (J/m^3), d_i is the thickness of layer i (m), R_i is the thermal resistance of layer i (Ks/J), $R_{sum,i}$ is the sum of thermal resistance above layer i (Ks/J). R_i is defined as

$$R_i = d_i / k_{unf,i}$$

where $k_{unf,i}$ is the unfrozen thermal conductivity (W $\cdot$ m^{-1} $\cdot$ K^{-1}) of layer i, which is calculated following the method of *Johansen* [1975]:

$$k_{unf,i} = (k_{sat,i} - k_{dry,i}) K_e + K_{dry,i}$$

where K_e is Kersten number, which is related to soil water content. The parameters $k_{sat,i}$ and $k_{dry,i}$ are saturated and dry thermal conductivities of a soil layer, which are specified for each soil layer type.

[78] If $dd_{need,i}$ is less than dd_{left}, the frozen state is changed to unfrozen, and a thawing front is moved to the top of next layer, and dd_{left} is recalculated:

$$dd_{left} = dd_{left} - dd_{need,i}$$

$R_{sum,i}$ is then updated by adding the thermal resistivity of the current layer to the old value of $R_{sum,i}$ and the TDSA then proceeds to the next layer if it is not rock.

[79] If $dd_{need,i}$ is greater than dd_{left},

$$d_{part} = -k_{unf,i} R_{sum,i} + \sqrt{k_{unf,i}^2 R_{sum,i}^2 + \frac{2 k_{frz,i} dd_{left}}{\lambda \theta_i}}$$

where d_{part} is partial depth that can be thawed, and $k_{frz,i}$ is the frozen thermal conductivity of layer i (J/Kms). A thawing front will be created at a depth d_{part} relative to the top of layer i. dd_{left} is set to zero and the iteration stops.

[80] If a layer is unfrozen, the dd_{left} is kept unchanged, $R_{sum,i}$ is updated and the TDSA then proceeds to the next layer if the layer is not rock. After the movement of thawing front downward, the same procedure is used to adjust the deepest front upward.

E2. Temperatures of All Layers

[81] After the positions of FTFs are determined, the temperature of each layer will be updated. If there is no front in whole ground column, the temperature of each layer

will be updated by solving finite difference equations of all layers, with the derived ground surface temperature from air temperature as the top boundary condition. Because the heat flux around 50–100 m can neglected for a time period of centuries [*Nicolsky et al.*, 2007], we assumed a zero heat flux as the lower boundary condition. If there is one front in whole ground column, the layers above and below the front will be updated separately by solving two different sets of equations assuming no phase change. If there are two or more fronts in the whole soil column, the temperatures of layers above first front will be updated by solving the finite difference equation of layers above first front, and a similar method will be used to update temperatures below the last front. For layers between first and last front, the temperatures are assumed to be 0°C.

[82] The Crank-Nicholson scheme is used to solve the finite difference equations of ground temperatures. To keep the calculation stable, an adaptive step-size integration approach is used. The initial time step is a half day. After advancing one time step, if the change of a layer's temperature is greater than a specified threshold (0.1°C in this study), the time step will be halved. Iteration continues until the calculation covers a full day.

E2.1. Snow Thermal Conductivity

[83] Snow thermal conductivity k_{sn} ($W \times m^{-1} \times K^{-1}$) are calculated following *Goodrich* [1982]:

$$k_{sn} = 2.9 \times 10^{-6} \rho_{sn}^2$$

where ρ_{sn} is the snow density in unit of $kg \times m^{-3}$, and the value of ρ_{sn} ranges from new snow density $\rho_{sn,new}$ to maximum snow density $\rho_{sn,\max}$ following *Verseghy* [1991], with a time step of 1 day:

$$\rho_{sn} = (\rho_{sn} - \rho_{sn,\max}) e^{-\tau} + \rho_{sn,\max}$$

where $\tau = 0.24$ corresponds to an e-folding time of about 4 days. $\rho_{sn,new}$ is specified to be 100 $kg \times m^{-3}$, while $\rho_{sn,\max}$ is the maximum snow density, which is specified to be 250 $kg \times m^{-3}$ for forest ecosystems [*Pomeroy et al.*, 1998] and 362 $kg \times m^{-3}$ for tundra ecosystems [*Ling and Zhang*, 2006].

E2.2. Soil Thermal Conductivity

[84] Soil thermal conductivity k_{sl} ($W \times m^{-1} \times K^{-1}$) is calculated following *Farouki* [1986]:

$$k_{sl} = \begin{cases} K_e k_{sl,sat} + (1 - K_e) k_{sl,dry} & S_r > 1 \times 10^{-7} \\ k_{sl,dry} & S_r \le 1 \times 10^{-7} \end{cases}$$

where K_e is Kersten number, and S_r is soil wetness. The parameters $k_{sl,sat}$, which is the saturated thermal conductivity, and $k_{sl,dry}$, which is the dry thermal conductivity, are calculated as:

$$k_{sl,sat} = k_{solid}^{1-\theta_{sat}} k_{liq}^{\theta_{liq}} k_{ice}^{\theta_{lice}},$$

and

$$k_{sl,dry} = k_{solid}^{1-\theta_{sat}} k_{air}^{\theta_{sat}}$$

where k_{solid}, k_{liq}, k_{ice}, and k_{air} are thermal conductivity of solid material, liquid, ice, and air, respectively. The parameters θ_{sat}, θ_{liq}, and θ_{ice} are porosity, volumetric liquid content, and volumetric ice content, respectively. The parameters k_{solid} and θ_{sat} are specified for each type of soil following *Beringer et al.* [2001]. In some cases, the simulated k_{sl} is too small for topsoil layers under very dry conditions. Therefore, the minimum thermal conductivity has been set 0.1 $W\ m^{-1}\ K^{-1}$ following *Hinzman et al.* [1991] to account for nonconductive heat exchange.

E2.3. Rock Thermal Conductivity

[85] The thermal conductivity of rock may vary by as much as a factor of two or three for the same type of rock. Because sedimentary rock underlies 72.9% of Alaska [*Peucker-Ehrenbrink and Miller*, 2003], we used a mean value of 2 $W \times m^{-1} \times K^{-1}$, the thermal conductivity of bedrock following *Clauser and Huenges* [1995].

E3. Volumetric Thermal Capacity

[86] The volumetric thermal capacity ($J \times m^{-3} \times K^{-1}$) is calculated based on the specific heat capacity ($J \times kg^{-1} \times K^{-1}$) and bulk density ($kg \times m^{-3}$). The specific heat capacities of soil are related to soil type, that of snow is 2117.27 $J \times kg^{-1} \times K^{-1}$, and that of rock is 1000 $J \times kg^{-1} \times K^{-1}$. The bulk densities of soil are related to soil type, the bulk density of snow is calculated during simulation, and the bulk density of rock is set to 2700 $kg \times m^{-3}$.

[87] **Acknowledgments.** We thank Dan Hayes of the Institute of Arctic Biology, who provided many of the driving data sets, and Xingang Fan, who provided station precipitation data that were corrected for bias. We also thank Eugenie Euskirchen, Qianlai Zhuang, two anonymous reviewers, and the associate editor for very thoughtful reviews of previous versions of this paper. This study was supported through grants provided as part of the One Hundred People Plan of Chinese Academy of Sciences, the North American Carbon Program (NASA NNG05GD25G), the Arctic System Science Program (NSF OPP-0531047 and OPP-0327664) the Bonanza Creek Long-term Ecological Program (funded jointly by NSF grant DEB-0423442 and USDA Forest Service, Pacific Northwest Research Station grant PNW01-JV11261952-231), and the USGS Fate of Carbon in Alaskan Landscapes (FOCAL) Project.

References

ACIA (2004), *Arctic Climate Impact Assessment*, Cambridge Univ. Press, Cambridge, U. K.

Balshi, M. S., et al. (2007), Role of fire disturbance in the carbon dynamics of the pan-boreal region: A process-based analysis, *J. Geophys. Res.*, *112*, G02029, doi:10.1029/2006JG000380.

Beringer, J., A. H. Lynch, F. Stuart Chapin III, M. Mack, and G. B. Bonan (2001), The representation of Arctic soils in the land surface model: The importance of mosses, *J. Clim.*, *14*, 3324–3335.

Beringer, J., S. F. Chapin, C. C. Thompson, and A. D. McGuire (2005), Surface energy exchanges along a tundra-forest transition and feedbacks to climate, *Agric. For. Meteorol.*, *131*, 143–161.

Bisbee, K. E., S. T. Gower, J. M. Norman, and E. V. Nordheim (2001), Environmental controls on ground cover species composition and productivity in a boreal black spruce forest, *Oecologia*, *129*, 261–270.

Bonan, G. B. (1996), A land surface model (LSM Version 1.0) for ecological, hydrological, and atmospheric studies: Technical description and users guide, *NCAR Tech. Note Tn-417+STR*, Natl. Cent. for Atmos. Res., Univ. Corp. for Atmos. Res., Boulder, Colo.

Bond-Lamberty, B., C. Wang, and S. T. Gower (2005), Spatiotemporal measurement and modeling of stand-level boreal forest soil temperatures, *Agric. For. Meteorol.*, *131*, 27–40.

Bond-Lamberty, B., S. T. Gower, and D. E. Ahl (2007), Improved simulation of poorly drained forests using Biome-BGC, *Tree Physiol.*, *27*, 703–715.

Brown, J., K. M. Hinkel, and F. E. Nelson (2000), The Circumpolar Active Layer Monitoring (CALM) Program: Research designs and Initial results, *Polar Geogr.*, *24*, 165–258.

Clapp, R. B., and M. G. Hornberger (1978), Empirical equations for some soil hydraulic properties, *Water Resour. Res.*, *14*, 601–604.

Clauser, C., and E. Huenges (1995), Thermal conductivity of rocks and minerals, in *Rocks Physics and Phase Relations: A Handbook of Physical Constants*, *AGU Ref. Shelf*, vol. 3, edited by T. Ahrens, pp. 105–126, AGU, Washington, D. C.

Cosby, J. B., M. G. Hornberger, R. B. Clapp, and T. R. Ginn (1984), A statistical exploration of the relationships of soil moisture characteristics to the physical properties of soils, *Water Resour. Res.*, *20*, 682–690.

Davidson, E. A., and I. A. Janssens (2006), Temperature sensitivity of soil carbon decomposition and feedbacks to climate change, *Nature*, *440*, 165–173.

Dunn, A. L., C. C. Barford, S. C. Wofsy, M. L. Goulden, and B. C. Daube (2007), A long-term record of carbon exchange in a boreal black spruce forest: Means, responses to interannual variability, and decadal trends, *Global Change Biol.*, *13*, 577–590.

Euskirchen, S. E., et al. (2006), Importance of recent shifts in soil thermal dynamics on growing season length, productivity, and carbon sequestration in terrestrial high-latitude ecosystems, *Global Change Biol.*, *12*, 731–750.

Farouki, O. T. (1986), Thermal properties of soils, Cold Reg. Res. and Eng. Lab., Hanover, N. H.

Friend, D. A., J. Schulz, and S. W. Running (1993), A physiology-based gap model of forest dynamics, *Ecology*, *74*, 792–797.

Goodrich, L. E. (1982), The influence of snow cover on the ground thermal regime, *Can. Geotech. J.*, *19*, 421–432.

Goulden, M. L., et al. (1998), Sensitivity of boreal forest carbon balance to soil thaw, *Science*, *279*, 214–216.

Harden, J., S. E. Trumbore, B. J. Stocks, A. I. Hirsch, S. T. Gower, K. P. O. Neill, and E. Kasischke (2000), The role of fire in the boreal carbon budget, *Global Change Biol.*, *6*, suppl. 1, 174–184.

Harden, J., K. L. Manies, M. R. Turetsky, and J. C. Neff (2006), Effects of wildfire and permafrost on soil organic matter and soil climate in interior Alaska, *Global Change Biol.*, *12*, 2391–2403.

Hayes, D. J., A. D. McGuire, D. W. Kicklighter, T. J. Burnside, and J. M. Melillo (2009), The effects of land cover and land use change on the contemporary carbon balance of the arctic and boreal ecosystems of northern Eurasia, in *Arctic Land Cover and Land Use in a Changing Climate*, edited by G. Gutman, chap. 5, Springer, New York, in press.

Hinzman, L. D., D. L. Kane, R. E. Gieck, and K. R. Everett (1991), Hydrologic and thermal properties of the active layer in the Alaskan arctic, *Cold Reg. Sci. Technol.*, *19*, 95–110.

Johansen, O. (1975), Thermal conductivity of soils, Ph.D. thesis, Univ. of Trondheim, Trondheim, Norway.

Johnstone, J. F., and E. Kasischke (2005), Stand-level effects of soil burn severity on postfire regeneration in a recently burned black spruce forest, *Can. J. For. Res.*, *35*, 2151–2163.

Ju, W., and J. Chen (2008), Simulating the effects of past changes in climate, atmospheric composition, and fire disturbance on soil carbon in Canada's forests and wetlands, *Global Biogeochem. Cycles*, *22*, GB3010, doi:10.1029/2007GB002935.

Kanamitsu, M., et al. (2002), NCEP-DOE AMIP-II Reanalysis (R-2), *Bull. Am. Meteorol. Soc.*, *83*, 1631–1643.

Karunaratne, K. C., and C. R. Burn (2004), Relations between air and surface temperature in discontinuous permafrost terrain near Nayo, Yukon Territory, *Can. J. Earth Sci.*, *41*, 1437–1451.

Kasischke, E., L. L. Bourgeau-Chavez, and J. F. Johnstone (2007), Assessing spatial and temporal variations in surface soil moisture in fire-disturbed black spruce forests in Interior Alaska using spaceborne synthetic aperture radar imagery—Implications for postfire tree recruitment, *Remote Sens. Environ.*, *108*, 42–58.

Kim, Y., M. Ueyama, F. Nakagawa, U. Tsunogai, Y. Harazono, and N. Tanaka (2007), Assessment of winter fluxes of CO_2 and CH_4 in boreal forest soils of central Alaska estimated by the profile method and the chamber method: A diagnosis of methane emission and implications for the regional carbon budget, *Tellus, Ser. B*, *59*, 223–233.

Klene, A. E., F. E. Nelson, and N. I. Shiklomanov (2001), The n factor as a tool in geocryological mapping: Seasonal thaw in the Kuparuk River basin, Alaska, *Phys. Geogr.*, *22*, 449–466.

Letts, M. G., N. T. Roulet, N. T. Comer, M. R. Skarupa, and D. L. Verseghy (2000), Parametrization of peatland hydraulic properties for the Canadian Land Surface Scheme, *Atmos. Ocean*, *38*, 141–160.

Liljedahl, A., L. D. Hinzman, R. Busey, and K. Yoshikawa (2007), Physical short-term changes after a tussock tundra fire, Seward Peninsula, Alaska, *J. Geophys. Res.*, *112*, F02S07, doi:10.1029/2006JF000554.

Ling, F., and T. Zhang (2006), Sensitivity of ground thermal regime and surface energy fluxes to tundra snow density in northern Alaska, *Cold Reg. Sci. Technol.*, *44*, 121–130.

Liu, H., and J. T. Randerson (2008), Interannual variability of surface energy exchange depends on stand age in a boreal forest fire chronosequence, *J. Geophys. Res.*, *113*, G01006, doi:10.1029/2007JG000483.

Liu, Y. (1996), Modeling the emissions of nitrous oxide (N_2O) and methane (CH_4) from the terrestrial biosphere to the atmosphere, Ph.D. thesis, 219 pp., Mass. Inst. of Technol., Cambridge.

Manies, K., J. Harden, K. Yoshikawa, and J. Randerson (2001), The effect of soil drainage on fire and carbon cycling in central Alaska, *U.S. Geol. Surv. Prof. Pap.*, *1678*.

Manies, K. L., J. W. Harden, K. Yoshikawa, and J. Randerson (2003), The impact of soil drainage on fire and carbon cycling in central Alaska, in *Studies by the U.S. Geological Survey in Alaska*, edited by J. Galloway, *U.S. Geol. Surv. Prof. Pap.*, *1678*, 24 pp.

Manies, K., J. Harden, S. Silva, P. H. Briggs, and B. M. Schmid (2004), Soil data from Picea mariana stands near Delta Junction, Alaska of different ages and soil drainage types, *U.S. Geol. Surv. Open File Rep.*, 2004–1271, 19 pp.

Manies, K. L., J. W. Harden, and H. Veldhuis (2006), Soil data from a moderately well and somewhat poorly drained fire chronosequence near Thompson, Manitoba, Canada, *U.S. Geol. Surv. Open File Rep.*, 2006–1291, 13 pp.

McGuire, A. D., et al. (2008), The Western Arctic Linkage Experiment (WALE): Overview and synthesis, *Earth Interact.*, *12*, doi:10.1175/2008EI239.1.

Mitchell, T. D., and P. D. Jones (2005), An improved method of constructing a database of monthly climate observations and associated high-resolution grids, *Int. J. Climatol.*, *25*, 693–712.

Nicolsky, D. J., V. E. Romanovsky, V. A. Alexeev, and D. M. Lawrence (2007), Improved modeling of permafrost dynamics in a GCM land-surface scheme, *Geophys. Res. Lett.*, *34*, L08501, doi:10.1029/2007GL029525.

Oelke, C., T. Zhang, and M. C. Serreze (2004), Modeling evidence for recent warming of the Arctic soil thermal regime, *Geophys. Res. Lett.*, *31*, L07208, doi:10.1029/2003GL019300.

Oleson, K. W., et al. (2004), Technical description of the Community Land Model (CLM), *NCAR Tech. Note TN-461+STR*, Natl. Cent. for Atmos. Res., Univ. Corp. for Atmos. Res., Boulder, Colo.

Overduin, P. P., K. Yoshikawa, D. L. Kane, and J. Harden (2005), Comparing electronic probes for volumetric water content of low-density feathermoss, *Sensor Rev.*, *25*, 215–221.

Peucker-Ehrenbrink, B., and M. W. Miller (2003), Quantitative bedrock geology of Alaska and Canada, *Geochem. Geophys. Geosyst.*, *4*(4), 8005, doi:10.1029/2002GC000449.

Pomeroy, J. W., M. D. Gray, R. K. Shook, B. Toth, R. Essery, A. Pietroniro, and N. Hedstrom (1998), An evaluation of snow accumulation and ablation processes for land surface modeling, *Hydrol. Process.*, *12*, 2339–2367.

Raich, J. W., E. B. Rastetter, J. Melillo, D. Kicklighter, P. A. Steudler, B. J. Peterson, A. L. Grace, B. Moore, and C. J. Vorosmarty (1991), Potential net primary productivity in South America: Application of a global model, *Ecol. Appl.*, *1*, 399–429.

Rastetter, E. B. (1996), Validating models of ecosystem response to global change, *BioScience*, *46*, 190–198.

Robinson, C. H. (2002), Controls on decomposition and soil nitrogen availability at high latitudes, *Plant Soil*, *242*, 65–81.

Roesh, A., M. Wild, H. Gilgen, and A. Ohmura (2001), A new snow cover fraction parameterization for the ECHAM4 GCM, *Clim. Dyn.*, *17*, 933–946.

Ruess, R. W., R. L. Hendrick, J. G. Vogel, and B. Sveinbjornsson (2006), The role of fine roots in the functioning of boreal forests, in *Alaska's Changing Boreal Forest*, edited by F. S. Chapin III et al., pp. 189–210, Oxford Univ. Press, New York.

Shanley, J. B., and A. Chalmers (1999), The effect of frozen soil on snowmelt runoff at Sleepers River, Vermont, *Hydrol. Process.*, *13*, 1843–1857.

Sitch, S., et al. (2003), Evaluation of ecosystem dynamics, plant geography and terrestrial carbon cycling in the LPJ dynamic global vegetation model, *Global Change Biol.*, *9*, 161–185.

Tarnocai, C. (2000), Carbon pools in soils of the Arctic, Subarctic and boreal regions of Canada, in *Global Climate Change and Cold Regions Ecosystems*, *Adv. Soil Sci.*, edited by R. Lal, J. M. Kimble, and B. A. Stewart, pp. 91–103, Lewis, Boca Raton, Fla.

van Cleve, K., C. T. Dyrness, L. A. Viereck, J. F. Fox, F. S. Chapin III, and W. Oechel (1983), Taiga ecosystems in interior Alaska, *BioScience*, *33*, 39–44.

van Wijk, T. M., M. Williams, J. A. Laundre, and G. R. Shaver (2003), Interannual variability of plant phenology in tussock tundra: Modelling interactions of plant productivity, plant phenology, snowmelt and soil thaw, *Global Change Biol.*, *9*, 743–758.

Verseghy, D. L. (1991), CLASS-A Canadian Land Surface Scheme for GCMs. I: Soil model, *Int. J. Climatol.*, *11*, 111–133.

Waring, R. H., and S. W. Running (1998), *Forest Ecosystems: Analysis at Multiple Scales*, Academic, San Diego, Calif.

White, M. A., P. Thornton, S. W. Running, and R. R. Nemani (2000), Parameterization and sensitivity analysis of the BIOM-BGC terrestrial ecosystem model: Net primary production controls, *Earth Interact.*, *4*, 1–85.

Wickland, K. P., and J. C. Neff (2007), Decomposition of soil organic matter from boreal black spruce forest: Environmental and chemical controls, *Biogeochemistry*, *87*, 29–47, doi:10.1007/s10533-007-9166-3.

Wilson, K. B., et al. (2002), Energy balance closure at FLUXNET sites, *Agric. For. Meteorol.*, *113*, 223–243.

Woo, M.-K., A. M. Arain, M. Mollinga, and S. Yi (2004), A two-directional freeze and thaw algorithm for hydrologic and land surface modeling, *Geophys. Res. Lett.*, *31*, L12501, doi:10.1029/2004GL019475.

Yang, D., D. L. Kane, Z. Zhang, D. Legates, and B. Goodison (2005), Bias corrections of long-term (1973–2004) daily precipitation data over the northern regions, *Geophys. Res. Lett.*, *32*, L19501, doi:10.1029/2005GL024057.

Yi, S., A. M. Arain, and M.-K. Woo (2006), Modifications of a land surface scheme for improved simulation of ground freeze-thaw in northern environments, *Geophys. Res. Lett.*, *33*, L13501, doi:10.1029/2006GL026340.

Yi, S., M.-K. Woo, and A. M. Arain (2007), Impacts of peat and vegetation on permafrost degradation under climate warming, *Geophys. Res. Lett.*, *34*, L16504, doi:10.1029/2007GL030550.

Yi, S., K. Manies, J. Harden, and A. D. McGuire (2009), The characteristics of organic soil in black spruce forests: Implications for the application of land surface and ecosystem models in cold regions, *Geophys. Res. Lett.*, *36*, L05501, doi:10.1029/2008GL037014.

Yoshikawa, K., P. P. Overduin, and J. Harden (2004), Moisture content measurement of moss (Sphagnum spp.) using commercial sensors, *Hydrol. Process.*, *15*, 309–318.

Zhang, Y., C. Li, C. C. Trettin, H. Li, and G. Sun (2002), An integrated model of soil, hydrology, and vegetation for carbon dynamics in wetland ecosystems, *Global Biogeochem. Cycles*, *16*(4), 1061, doi:10.1029/2001GB001838.

Zhuang, Q., V. E. Romanovsky, and A. D. McGuire (2001), Incorporation of a permafrost model into a large-scale ecosystem model: Evaluation of temporal and spatial scaling issues in simulating soil thermal dynamics, *J. Geophys. Res.*, *106*(D24), 33,649–33,670.

Zhuang, Q., A. D. McGuire, J. Harden, K. P. O'Neill, V. E. Romanovsky, and J. Yarie (2002), Modeling soil thermal and carbon dynamics of a fire chronosequence in interior Alaska, *J. Geophys. Res.*, *107*, 8147, doi:10.1029/2001JD001244 [printed *108*(D1), 2003].

Zhuang, Q., et al. (2003), Carbon cycling in extratropical terrestrial ecosystems of the Northern Hemisphere during the 20th century: A modeling analysis of the influences of soil thermal dynamics, *Tellus, Ser. B*, *55*, 751–776.

Zhuang, Q., J. Melillo, D. Kicklighter, R. G. Prinn, A. D. McGuire, P. A. Steudler, B. S. Felzer, and S. Hu (2004), Methane fluxes between terrestrial ecosystems and the atmosphere at northern high latitudes during the past century: A retrospective analysis with a process-based biogeochemistry model, *Global Biogeochem. Cycles*, *18*, GB3010, doi:10.1029/2004GB002239.

J. Harden and K. Manies, U.S. Geological Survey, Menlo Park, CA 94025, USA.

L. Hinzman, Y. Kim, and A. Liljedahl, International Arctic Research Center, University of Alaska Fairbanks, Fairbanks, AK 99775, USA.

E. Kasischke, Department of Geography, University of Maryland, 2181 LeFrak Hall, College Park, MD 20742, USA.

H. Liu, Department of Physics, Atmospheric Sciences and General Sciences, Jackson State University, Jackson, MS 39217, USA.

S. Marchenko and V. Romanovsky, Geophysical Institute, University of Alaska Fairbanks, Fairbanks, AK 99775, USA.

A. D. McGuire, Alaska Cooperative Fish and Wildlife Research Unit, U.S. Geological Survey, University of Alaska Fairbanks, Fairbanks, AK 99775, USA.

J. Randerson, Department of Earth System Science, University of California, Irvine, CA 92697, USA.

S. Yi, State Key Laboratory of Cryosphere Sciences, Cold and Arid Regions Environmental and Engineering Institute, Chinese Academy of Sciences, Lanzhou, Gansu 730000, China. (yishuhua@gmail.com)